

## Monthly element/Ca trends and inter chamber variability in two planktic Foraminifera species: *Globigerinoides ruber albus* and *Turborotalita clarkei* from a hypersaline oligotrophic sea

Noy Levy<sup>1,2</sup>, Adi Torfstein<sup>1,3</sup>, Ralf Schiebel<sup>2</sup>, Natalie Chernihovsky<sup>1,3</sup>, Klaus Peter Jochum<sup>2</sup>, Ulrike Weis<sup>2</sup>, Brigitte Stoll<sup>2</sup>, Gerald H. Haug<sup>2,4</sup>

- 1) The Fredy & Nadine Herrmann Institute of Earth Sciences, Hebrew University of Jerusalem, Jerusalem 91904, Israel.
- 2) Max Planck Institute for Chemistry, Hahn-Meitner-Weg 1, 55128 Mainz, Germany.
- 3) Interuniversity Institute for Marine Sciences, Eilat 88103, Israel.
- 4) Department of Earth Sciences, ETH Zurich, Sonneggstrasse 5, 8092 Zurich, Switzerland

 Deceased, November 9, 2024

Correspondence to: Noy Levy (noy.levy2@mail.huji.ac.il)

## Abstract

Environmental and biological factors influence the trace element composition (element/Ca) of planktic foraminifer shells. Consequently, the element/Ca measured in these shells (tests) are utilized as proxies to reconstruct past oceanic and climatic conditions. As single shell analyses are increasingly used in paleoceanographic research it is important to understand how proxy systematics change between species, individuals of the same species in a given population, and among chambers of a single individual during its life cycle. Here we present a time series of the chemical composition of planktic foraminifers retrieved using sediment traps between June 2014 and June 2015 at the northern part of the Gulf of Aqaba (aka Gulf of Eilat). Laser ablation ICP-MS element/Ca measurements were performed on single shells and chambers of *Globigerinoides ruber albus* and *Turborotalita clarkei*, collected monthly from five water depths (120 m, 220 m, 350 m, 450 m, and 570 m). Sediment trap samples were paired with corresponding data on water column hydrography and chemistry. Pooled means of measured element/Ca display species-specific and element-specific behavior, with generally higher

34 values for *T. clarkei* phenotypes ('big' and 'encrusted') in comparison to *G. ruber albus*. Some  
35 element/Ca values measured in water column specimens, such as Al/Ca, vary significantly  
36 from core-top specimens. A unique finding is a prominent increase in element/Ca around  
37 March-April 2015, during maximum water column mixing, mostly apparent in *T. clarkei* and  
38 to a lesser extent in *G. ruber albus*. This spring element/Ca increase is observed in most  
39 measured elements and is further associated with an increase in inter-chamber variability  
40 (ICV). Inter-chamber element/Ca patterns show element enrichment/depletion in the most  
41 recently precipitated (final, F0) chamber in comparison to the older chambers (penultimate (F-  
42 1), antepenultimate (F-2), etc.). Element/Ca in F0 may also be less sensitive to surrounding  
43 environmental conditions. For example, the Mg/Ca of the F-1 and F-2 chambers of *G. ruber*  
44 *albus* display a positive relationship with mixed layer temperatures while F0 does not. To  
45 overcome this effect, we suggest using pooled means from non-F0 fractions as environmental  
46 records and paleo proxies.

47 These results highlight the complexity of proxy systematics that rises from the variability in  
48 element/Ca measured among different species and between chambers, caused by ecological  
49 conditions and other processes in the water column including physical, chemical, and  
50 biological effects.

51

52 1. Introduction

53 1.1 Planktic foraminifera as traces of the past environment

54 Planktic Foraminifera (PF) shells are useful archives for studying the history of Earth's  
55 climate and oceans, as their calcareous shells reflect the environmental conditions during their  
56 formation (Berggren et al., 1995; Rosenthal, 2007; Schiebel & Hemleben, 2017; Kucera, 2007;  
57 Katz et al., 2010; Gupta, 1999; Davis et al., 2020.). Various element/Ca measured in PF tests  
58 have been linked to ambient seawater temperature (e.g., Mg/Ca; Nurenb erg et al., 1996;  
59 Rosenthal et al., 2004), salinity (e.g., Na/Ca; Mezger et al., 2016; Gray et al., 2023), the  
60 carbonate system (e.g., B/Ca; Babila et al., 2014; Henehan et al., 2015; Haynes et al., 2019),  
61 productivity (e.g., Ba/Ca; Fritz-Enders et al., 2022), and chemical weathering (e.g., Ti/Ca;  
62 Amaglio et al., 2025.). In the past, the use of these proxies relied on bulk analysis of the entire  
63 shell or multiple shells. However, although first attempts in single chamber LA-ICP-MS started  
64 back in 2003 (Eggins et al., 2003; Reichart et al., 2003), only in recent years there has been an  
65 increase in the use of high-resolution analytical techniques, such as Laser Ablation (LA) ICP-

**Deleted:** and others

**Deleted:** closely

**Deleted:** pH and

**Deleted:** , among others

70 MS and electron microprobe analyses in paleoceanographic studies (Davis et al., 2020). The  
71 element/Ca measurements of single specimens (Individual Foraminifer Analysis, IFA)  
72 revealed high variability between individuals of the same population as well as significant  
73 intra-shell variability (i.e., inter chamber variability, ICV) (Sadekov et al., 2008; Fehrenbacher  
74 et al., 2020; Hupp & Fehrenbacher, 2024; Fischer et al., 2024; Davis et al., 2020, and references  
75 therein). Despite the analytical advancements, the variations in the geochemical signatures of  
76 PF shells are poorly understood and, while they are likely related to the life cycles and  
77 reproductive modes of many species there are still knowledge gaps in our understanding of  
78 proxy systematics in single shell and single chamber of PF species. There is also a lack of  
79 detailed description and understanding of element/Ca systematics in description of small-sized  
80 species such as *T. clarkei*, which have been largely overlooked in previous studies despite their  
81 significant contribution to the settling PF tests (export flux), as observed in the northern Red  
82 Sea (Chernihovsky et al., 2018). Furthermore, specific marine regions, such as in oligotrophic,  
83 subtropical basins, particularly in deep-water environments, are not well-established in terms  
84 of their spatial and temporal dynamics (Schiebel & Hemleben, 2017).

## 85 1.2 Planktic Foraminifer population dynamics in The Gulf of Aqaba

86 The Gulf of Aqaba (GOA) is considered an open ocean proxy environment (Chase et al.,  
87 2011). It is an oligotrophic basin where the main lithogenic flux is derived from dust. During  
88 summer (April-September), a ~200 m deep thermocline separates nutrient-depleted surface  
89 waters (~25°C) from the nutrient-rich deep layer (~21°C). In winter, spring (October-April),  
90 the thermocline gradually erodes due to surface cooling (Figs. 1a and 1e; Meeder et al., 2012),  
91 which can lead to the development of a deep mixed layer. Although the depth of the mixed  
92 layer varies annually with climatic conditions, the long-term mean mixing depth is  
93 approximately 300-400 m, and deep mixing can extend to the sea floor while it typically  
94 reaches maximum depth by late March. The regional terrestrial climate is hyper-arid (mean  
95 annual rainfall <30 mm) and the main sources for terrigenous material to the GOA are dust  
96 storms originating from the Sahara and Arabian Deserts, as well as rare localized floods (Katz  
97 et al., 2015; Chase et al., 2011; Ganor et al., 2001; Torfstein et al., 2017).

**Deleted:** The

**Deleted:** associated changes

**Deleted:** despite the analytical advancements,

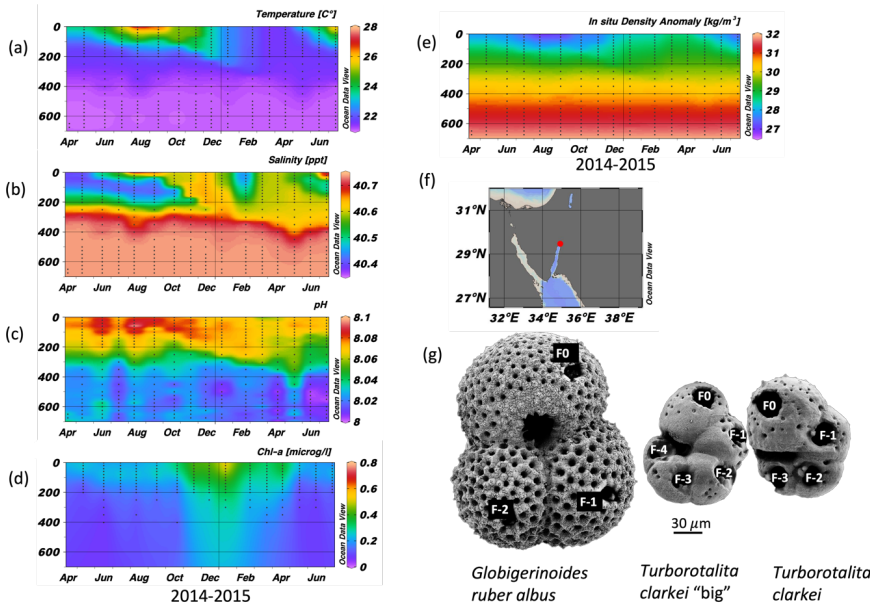
**Deleted:** although they are potentially related to the observed shell and chamber element/Ca variability, the life cycles and reproductive modes of many species, as they calcify their shell chambers one at a time

**Deleted:** proxy

**Deleted:** of the dynamics

**Deleted:** column

**Deleted:** /

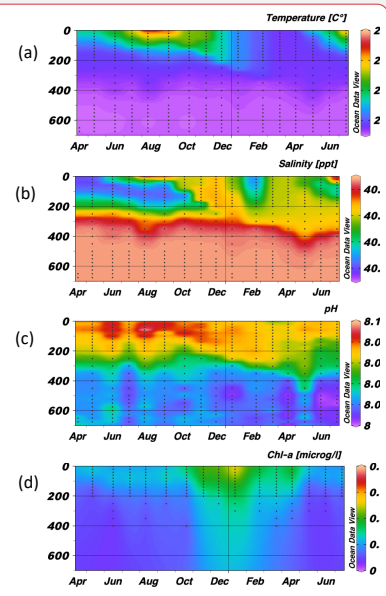


109  
110 Figure 1: Time series of temperature (a), salinity (b), pH (c), Chlorophyll-a concentration (d),  
111 and in situ density anomaly (e), measured in the Gulf of Aqaba between April 2014 and June  
112 2015 by the National Monitoring Program (NMP, Shaked & Genin, 2016). Y-axis is depth (m);  
113 A map of the Gulf of Aqaba (f); and (g) scanning electron micrographs of the three morpho-  
114 species (exhibiting ablation holes in each chamber (labelled), from Levy et al., 2023).  
115

116 Planktic foraminifera fluxes in the GOA demonstrate strong seasonality, with low fluxes  
117 during the summer months, gradually increasing during the autumn-winter, coeval with  
118 decreasing sea-surface temperatures and deepening of the mixed layer in the GOA that drives  
119 advection of nutrient-replete subsurface waters into the mixed layer (Fig. 2). This in turn  
120 triggers an increase in primary productivity, expressed by enhanced chlorophyll-a  
121 concentrations and higher PF fluxes (Chernihovsky et al., 2018, 2020).

122 Spinose species constitute the majority of the PF assemblage. The smaller size fraction,  
123 63-125  $\mu\text{m}$ , is 86% from the total flux and is dominated by *T. clarkei*. The 125-500  $\mu\text{m}$  size-  
124 fraction (~13 %) is dominated by the species *G. ruber albus*, while less than 1% of the shells  
125 are in the range of 500-1000  $\mu\text{m}$ , dominated by *O. universa* (Chernihovsky et al., 2018).

126 *Globigerinoides ruber albus* and *T. clarkei* inhabit different dwelling-depths and have  
127 different life strategies. *Globigerinoides ruber albus* is a surface dweller and is photo-symbiont

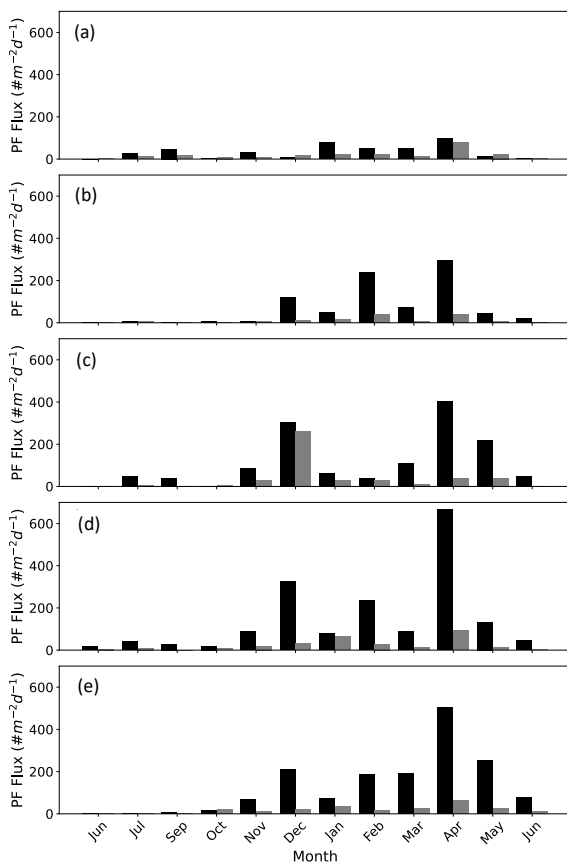


Deleted:  
Formatted

Deleted: diverse

130 bearing, while *T. clarkei* tends to dwell below the mixed layer depth and is barren of photo-  
 131 symbionts (Rebotim et al., 2017; Schiebel & Hemleben, 2017; Levy et al., 2023). Furthermore,  
 132 it has been suggested that *G. ruber albus* and *T. clarkei* do not share the same dietary  
 133 preferences: *G. ruber albus* being more carnivorous than the detritivorous *T. clarkei* which may  
 134 forage at the exported matter below the pycnocline (Schiebel & Hemleben, 2017). In the GOA,  
 135 *T. clarkei* has two phenotypes: *T. clarkei* ‘big’, with all of its test chambers are fully  
 136 recognizable and their surface is relatively smooth and *T. clarkei* ‘encrusted’ with a less smooth  
 137 shell surface and is smaller than the ‘big’ type (Levy et al., 2023).

Deleted: high



138  
 139 Figure 2: PF fluxes in the Gulf of Aqaba between June 2014 and June 2015 presented according  
 140 to the size fractions >63-125  $\mu\text{m}$  (black bars) and >125-500  $\mu\text{m}$  (grey bars) at the different  
 141 sediment trap depths a) 120 m, b) 220 m, c) 340 m, d) 450 m, and e) 570 m. Data from  
 142 Chernihovsky et al. (2018).

144 In this study, we investigate the range of element values, year-round trends and inter-  
145 chamber element/Ca variability in *G. ruber albus* and *T. clarkei* tests collected in sediment  
146 traps at various water column depths from the GOA. We assess whether the chambers record  
147 temporal-seasonal patterns, and the implications for using single chamber data for geochemical  
148 proxies (Mg/Ca, B/Ca, Na/Ca). Examining inter-chamber variability sheds light on how trace  
149 elements are incorporated during calcification, distinguishing physiological controls (e.g.,  
150 ontogenetic changes across successive chambers) from environmental influences such as  
151 temperature, salinity and nutrient availability. Using *G. ruber* and *T. clarkei* from the GOA  
152 provides a contrasting framework which together, these species enable us to refine element/Ca  
153 proxy calibrations across vertical gradients in the water column in a warm and hyper-saline  
154 oligotrophic environment.

155

## 156 2. Methodology

### 157 2.1. Sampling and oceanographic data

158 A bottom-tethered mooring has been deployed continuously since January 2014 near  
159 Station A, northern GOA ( $29^{\circ} 28'95' \text{ N}$ ,  $34^{\circ} 56'22' \text{ E}$ ,  $\sim 605 \text{ m}$  water depth) (Torfstein et al.,  
160 2020). Five KC Denmark cylinder sediment traps were mounted vertically and located at  
161 depths of 120 m, 220 m, 350 m, 450 m, and 570 m below the surface. The trap samples were  
162 collected at a monthly resolution. Furthermore, PF samples from the sediment interface were  
163 collected using a box core ('core top'). Further detailed description of the mooring, sampling,  
164 sample processing, and trapping efficiencies can be found in Chernihovsky et al. (2018) and  
165 Torfstein et al. (2020). Here, we report the findings derived from the PF tests collected between  
166 June 2014 and June 2015. Water column physical and chemical parameters are routinely  
167 collected at Station A by the Israel National Monitoring Program (NMP, Shaked & Genin,  
168 2016). This includes sea surface and water column temperature ( $^{\circ}\text{C}$ ), salinity, oxygen  
169 concentration ( $\mu\text{mol/l}$ ), alkalinity ( $\text{meq/kg}$ ),  $\text{pH}$ , and chlorophyll-a concentration ( $\mu\text{g/l}$ ). Mixed  
170 layer depth (MLD) was defined as the shallowest depth where the TEOS-10 potential density  
171 anomaly ( $\sigma_0$ ), computed with gsw from Practical Salinity and in-situ temperature with pressure  
172 from depth at Station A, exceeded a near-surface reference by  $\Delta\sigma_0 = 0.03 \text{ kg m}^{-3}$ ; the reference  
173 density was the median  $\sigma_0$  within 0–10 m (or the shallowest 10 m available when the surface  
174 was not sampled). Temperature, salinity, and  $\text{pH}$  within the mixed layer were then calculated  
175 as thickness-weighted means by linearly interpolating each profile onto a 0.5 m grid and  
176 averaging from the surface to the MLD.

**Deleted:** Understanding inter-chamber variability sheds light on biomineralization processes and environmental factors that occur during different stages of the organism's life cycle. This in turn improves the calibration of element/Ca as proxies for reliable reconstruction of past oceanic and climatic conditions. Focusing on PF from the GOA provides critical insights into the use of foraminiferal element/Ca as proxies in a ...

**Deleted:** ¶

**Formatted:** Font colour: Text 1

**Formatted:** Outline numbered + Level: 1 + Numbering Style: 1, 2, 3, ... + Start at: 1 + Alignment: Left + Aligned at: 0.63 cm + Indent at: 1.27 cm

**Deleted:**

**Deleted:** The mixed layer depth (MLD) is defined as the water depth where the density anomaly ( $\sigma_0$ ) is equal to, or above, the water density of the surface water column plus a density threshold of  $0.125 \text{ kg/m}^3$  (Sprintall & Tomczak, 1992)....

**Formatted:** Font: Italic, Complex Script Font: Italic

192        2.2. Species classification and preparation for LA-ICP-MS

193

194        We examined the shell chemical properties of two flux dominating PF species *T. clarkei*  
195 and *G. ruber albus* (i.e., sensu stricto, white). For *T. clarkei* we examined two morphotypes:  
196 ‘big’ and ‘encrusted’. Identification and nomenclature of the PF taxa followed Schiebel &  
197 Hemleben (2017), Morard et al. (2019), and Brummer & Kucera (2022). Three individuals  
198 were picked from each sediment trap depth during each month between June 2014 and June  
199 2015. Preliminary preparation and cleaning steps are detailed by Chernihovsky et al. (2018).  
200 Reductive and oxidative cleaning had been avoided to retain original signals related to the  
201 different encrustation processes and preserve all calcite layers added to the shell during  
202 ontogeny (Schiebel & Hemleben, 2017; Jochum et al., 2019). Specifically, the shell of *T.*  
203 *clarkei* is prone to loss of material during reductive and oxidative treatment as it has very thin  
204 chamber walls (ranging between 1.9 and 3.6  $\mu\text{m}$ ; Levy et al., 2023). Single chamber  
205 measurements were performed to asses inter chamber variability (ICV), on individual shells  
206 (individual foraminifer analysis; IFA) using Laser Ablation Inductively Coupled Plasma Mass  
207 Spectrometry (LA-ICP-MS). We measured 156 specimens in total and 615 chambers; 57  
208 individuals (168 chambers) of *G. ruber albus*, 52 individuals (242 chambers) of *T. clarkei* ‘big’  
209 and 48 individuals (204 chambers) of *T. clarkei* ‘encrusted’. Samples were glued to glass slides  
210 using a methyl-hydroxy-propyl-cellulose (MHPC 1:100), positioned with the umbilical side  
211 up.

212

213        2.3. LA-ICP-MS and data processing

214        Analyses of the calcium-normalized elements for B, Na, Mg, Al, Ti, Mn, Fe, Co, Sr, Ba,  
215 Nd, Pb, Th, and U were conducted using a 200 nm wavelength NWR femtosecond (fs) LASER  
216 system from ESI, combined with a sector-field Thermo Element-2 ICP mass spectrometer  
217 (Jochum et al., 2014). Measurements were performed using a 15 Hz pulse repetition rate (PRR),  
218 at low fluence (0.1–0.6 J/cm<sup>2</sup>), and 18 seconds dwelling time. A 30  $\mu\text{m}$  diameter spot size was  
219 selected, as it is the maximum diameter for analysis fitting in a single chamber of the small *T.*  
220 *clarkei*. The microanalytical synthetic reference material MACS-3 for carbonate, NIST-612,  
221 and NIST-610 were used for calibration. NIST-612 was used for the tuning of the ICP-MS  
222 (Jochum et al., 2019). The average element-to-calcium ratio from the spot derived LA-ICP-MS  
223 count data was calculated from count data immediately after the start of the ablation peak apex  
224 until the point identified as the termination of calcite based on the Mg/Ca profile. This time

**Deleted:** shells

**Deleted:** with a width

**Deleted:** -

**Deleted:** (

**Deleted:** on

**Deleted:** .

**Formatted:** Font: Italic, Complex Script Font: Italic

**Formatted:** Font: Italic, Complex Script Font: Italic

**Formatted:** Font: Italic, Complex Script Font: Italic

**Formatted:** Font: Not Italic, Complex Script Font: Not Italic

**Formatted:** Font: Not Italic, Complex Script Font: Not Italic

**Formatted:** Font: Not Italic, Complex Script Font: Not Italic

**Formatted:** Font: Not Italic, Complex Script Font: Not Italic

interval represents the stable internal material of the shell; excluding the noisy beginnings and ends of the ablation event. For *G. ruber* the mean ablation time length used for calculation was  $4.9 \pm 2.3$  secs, while for the smaller and thinner *T. clarkei* it was  $2.6 \pm 1.5$  secs and  $2.4 \pm 1.4$  secs, for ‘big’ and ‘encrusted’ types, respectively.

The measurement precision (1 relative standard deviation in percent; 1 RSD) yield uncertainties for references materials between ~ 5-17 % for the calcium-normalized elements (Supplementary table S1). Single spot measurements were made on each chamber of the individual shells. Chambers are labelled F0 (final chamber), F-1 (final minus one), F-2, and so on, for the penultimate, antepenultimate, and further chambers, respectively. We calculated averages and standard deviations of element/Ca of single individuals (calculated from all single chamber element/Ca in one shell) and relative standard errors of element/Ca of pooled measurements for a specific morphotype.

## 2.4 Statistical Analysis

We used redundancy analysis (RDA) to quantify how variation in shell element/Ca responses relates to environmental conditions (MLD, T, S, and pH). For each species, we assembled two time-aligned matrices by date: (i) a multivariate response matrix containing the element/Ca values at each sampled depth (120, 220, 340, 450, 570 m) plus the overall total, and (ii) an environmental matrix containing environmental predictors. RDA was fit using the vegan package in R (function rda), which is equivalent to multivariate multiple regression followed by PCA of the fitted values. Biplots were produced with arrows show the direction of increasing predictor values and their relative importance, and response points (depths/TOTAL) project positively or negatively onto each arrow according to their alignment, with the proportions of constrained variance carried by the first RDA axes (labels shown on the biplot axes). As a measure of specimen inter-chamber variability (ICV), the standard deviation (SD) was calculated for each individual. We calculated Spearman rank correlation matrices in R for each species across element/Ca and SD, together with environmental parameters, with the spearman correlation coefficients visualised as heatmaps (associated p-values reported in supplementary table's S2 and S3, respectively).

259

260 3. Results:

<b>Formatted:</b> Font: Not Italic, Complex Script Font: Not Italic
<b>Formatted:</b> Font: Not Italic, Complex Script Font: Not Italic
<b>Formatted:</b> Font: Not Italic, Complex Script Font: Not Italic
<b>Formatted:</b> Font: Not Italic, Complex Script Font: Not Italic
<b>Formatted:</b> Font: Not Italic, Complex Script Font: Not Italic
<b>Deleted:</b>
<b>Formatted:</b> Font: Not Italic, Complex Script Font: Not Italic

Deleted:

### Formatted: Justified

**Formatted:** Font: Italic, Complex Script Font: Italic

**Moved down [2]:** Depth-averaged values of element/Ca measured in *G. ruber albus* and *T. clarkei* shells using LA-ICP-MS ¶

Generally, the means of Mg/Ca, Sr/Ca, B/Ca, Na/Ca and Ba/Ca in *G. ruber albus* indicate that the composition of tests, from most water depths is similar to that of core-top samples (Figs. 3a-3d, 3j). In contrast, Al/Ca, Ti/Ca, Mn/Ca, Fe/Ca, Nd/Ca, Th/Ca, and U/Ca (Figs. 3e-3i, 3k, 3m, 3n) in the tests from sediment interface were higher than in the water column, and lower in case of Co/Ca and Pb/Ca (Figs. 3i, 3l).

**Deleted:** ¶

Formatted: Font colour: Auto, Highlight

**Formatted:** List Paragraph, Left, Outline numbered + Level: 1 + Numbering Style: 1, 2, 3, ... + Start at: 1 + Alignment: Left + Aligned at: 0.63 cm + Indent at: 1.27 cm

304

### 3.1. Shell-bound element/Ca time series trends in *G. ruber albus* and *T. clarkei* shells

305 Single chamber Mg/Ca over water column depths in *G. ruber albus* range between 2.01  
 306 mmol/mol (340 m; June 2015) and 18.49 mmol/mol (340 m; July-August 2014), with  
 307 lower/higher values during winter/summer months, respectively (Figs. 3b-3f). A unique  
 308 observation is an increase in Mg/Ca seen during spring (March-April), i.e., months with  
 309 maximum surface water column mixing, at some water depths (220 m, 340 m, 450 m; Figs. 3c-  
 310 3e). Accompanied with the Mg/Ca increase is a clear increase in ICV as evident by the  
 311 divergence of chamber values. The SD of *G. ruber albus* ranges between 0.14 in February 2015  
 312 at 450 m water depth and 7.27 during April 2015 at 120 m water depth. Generally, it appears  
 313 that Mg/Ca is lower in F0 chambers (orange dotted line) compared to preceding chambers,  
 314 especially during months with very shallow MLD (3a-3g). Mg/Ca in *T. clarkei* ‘big’ range  
 315 between 4.00 mmol/mol (340 m; June 2015) and 77.02 mmol/mol (220 m; March 2015) and  
 316 between 4.06 mmol/mol (570 m; December 2014) and 51.22 mmol/mol (120 m; April 2015)  
 317 in *T. clarkei* ‘encrusted’, respectively. For both *T. clarkei* ‘big’ and *T. clarkei* ‘encrusted’ there  
 318 are high excursions in all chambers during months of water column mixing while MLD is  
 319 deepest (circa April; 3j-3w). The SD ranges between 0.43 and 25.38 (120 m; September 2014  
 320 and, 220 m; April 2015 respectively) for *T. clarkei* ‘big’ and for *T. clarkei* ‘encrusted’ is up to  
 321 18.52 (340 m; March 2015).

322

**Moved down [1]:** Pooled mean values of Mg/Ca in *G. ruber albus* taken from all water column depths in the GOA reflect MLD temperatures (Fig. 10).

**Deleted:** 4

**Formatted:** Highlight

**Deleted:** 4a

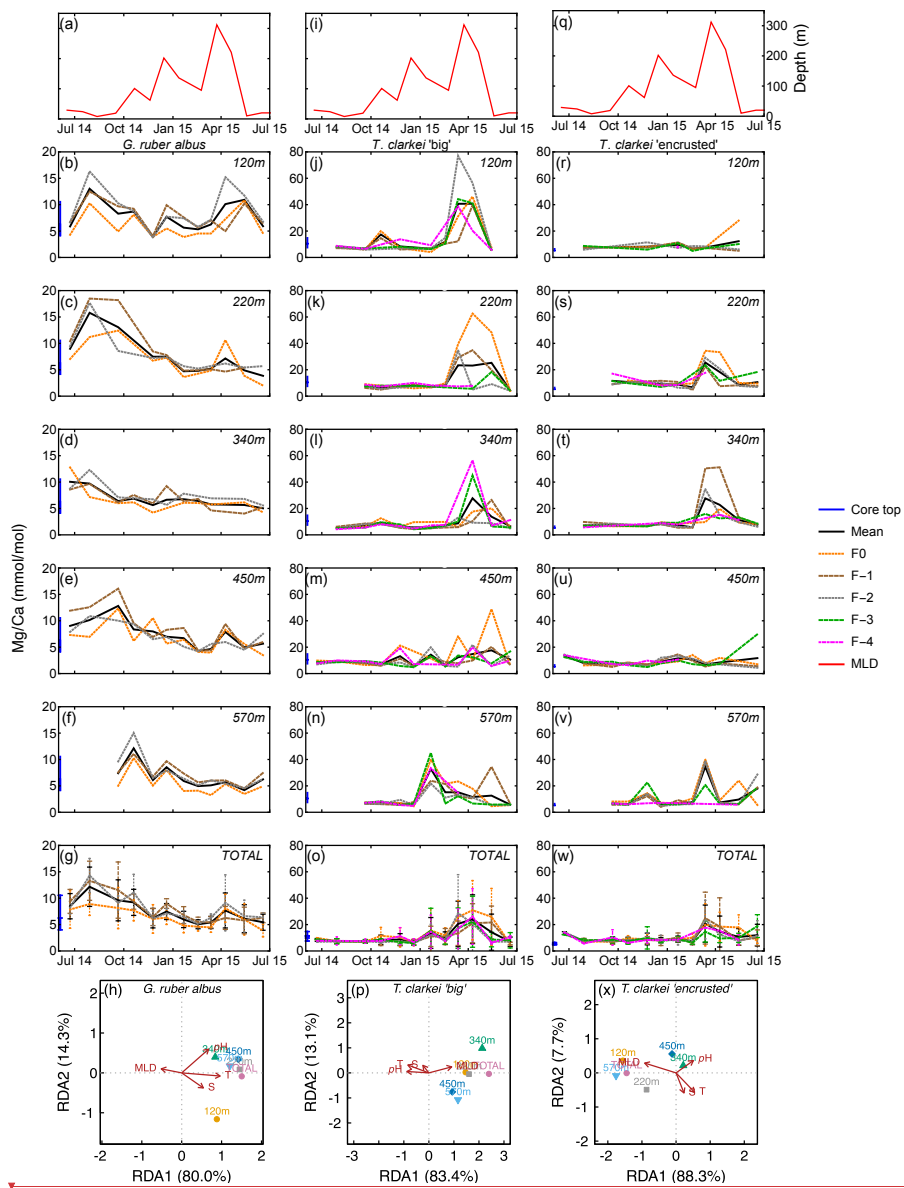
**Deleted:** 4e

**Deleted:** 4b

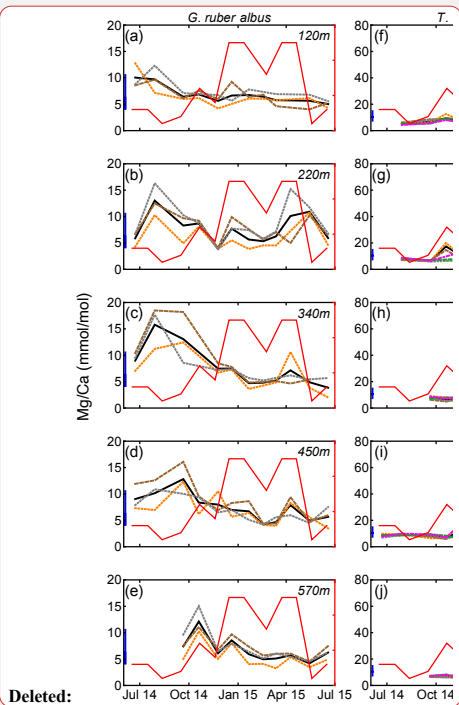
**Deleted:** 4d

**Formatted:** Font: Italic, Complex Script Font: Italic

**Deleted:**



332  
333 Figure 3: Time series of Mg/Ca values measured from the shells of *G. ruber albus* (b-f), *T.*  
334 *clarkei* 'big' (j-n) and *T. clarkei* 'encrusted' (r-v), derived from sediment traps located at  
335 different water depths (120-570 m). Mg/Ca of core top are marked by a blue bar along the left  
336 y-axes. Top panels a, i, and q show the depth (meters below surface layer) of the mixed layer



345 depth (MLD). Panels g, o, and w represent the average values of all depths for each chamber  
346 for each species. Panels h, p and x show the redundancy analysis (RDA) per species for each  
347 water depth with MLD depth, temperature, salinity and pH as explanatory variables.

Formatted: Font: Italic, Complex Script Font: Italic

349 The *G. ruber albus* RDA analysis of Mg/Ca show that most water depth samples, except for  
350 the 120 m are clustered together and align with temperature and MLD, positive and negative  
351 respectively. *Turborotalita clarkei* 'big' exhibits a contrasting image compared to *G. ruber*  
352 *albus* and positively correlates with MLD while negatively correlating with temperature,  
353 salinity, pH. All three morpho-species show a distinct dominance of RDA1 explaining >80%  
354 of the variance (Figs. 3h, 3p and 3x).

Formatted: Font: Italic, Complex Script Font: Italic

Formatted: Justified, Line spacing: 1.5 lines

Formatted: Font: Not Bold, Complex Script Font: Not Bold

Formatted: Font: Not Bold, Complex Script Font: Not Bold

Formatted: Font: Not Bold, Complex Script Font: Not Bold

Formatted: Font: Italic, Complex Script Font: Italic

Formatted: Font: Italic, Complex Script Font: Italic

Formatted: Font: Italic, Complex Script Font: Italic

Formatted

355 ▲  
356 Sr/Ca in *G. ruber albus* range between 1.25 mmol/mol (570 m; January 2015) and 2.27  
357 mmol/mol (340 m; November 2014) (Figs. 4b-4f). The SD in *G. ruber albus* ranges reaches up  
358 to 0.48 (220 m; November 2014). Single chamber Sr/Ca in *T. clarkei* 'big' range between 0.94  
359 mmol/mol (340 m; January 2015) and 2.76 mmol/mol (220 m; April 2015) and for *T. clarkei*  
360 'encrusted' between 0.54 mmol/mol (340 m; April 2015) and 2.92 mmol/mol (570 m; June  
361 2015), respectively (Figs. 4i-4n, and 4r-4v). *Turborotalita clarkei* 'big' and *T. clarkei*  
362 'encrusted' display more ICV than *G. ruber albus*, with peaking Sr/Ca in numerous chambers  
363 around April 2015 (Figs. 4j-4w). During the spring months of 2015, Sr/Ca values range  
364 between 1.45-2.04 mmol/mol in *G. ruber albus*, 1.32-2.76 mmol/mol in *T. clarkei* 'big' and  
365 0.54-2.27 mmol/mol in *T. clarkei* 'encrusted', respectively (Fig. 4; Fig. S1). Additionally, the  
366 SD of *T. clarkei* 'big' is the highest at 0.43 in March 2015 at 120 m water depth, and lowest at  
367 0.02 in June-July 2014, at 340 m water depth. For *T. clarkei* 'encrusted' SD reaches 0.7 (220  
368 m; April 2015). While the RDA analysis of *T. clarkei* 'big' show a high RDA1 dominance  
369 (91.6%), the RDA1 of *G. ruber albus* and *T. clarkei* 'encrusted' are lower (75.9% and 67.1%  
370 respectively). In both *G. ruber albus* and *T. clarkei* 'big' the environmental factors (pH, salinity  
371 and temperature) point together and opposite to MLD, while in *T. clarkei* 'encrusted' salinity  
372 and MLD are more closely related.

Deleted: 5a

Deleted: 5c

Formatted: Font: Italic, Complex Script Font: Italic

Deleted: 5f

Deleted: 5j

Deleted: 5k

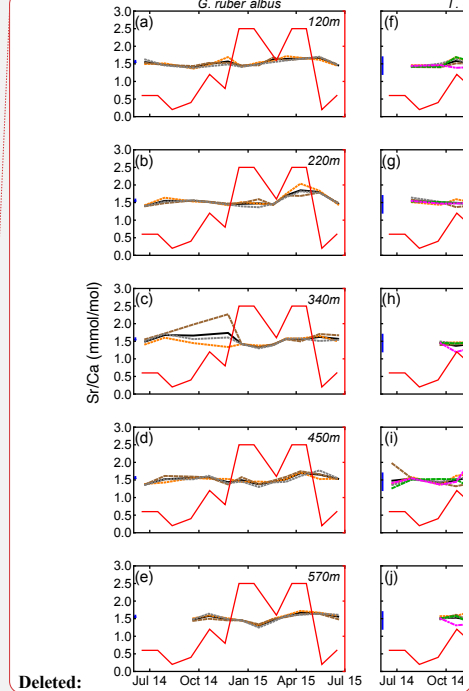
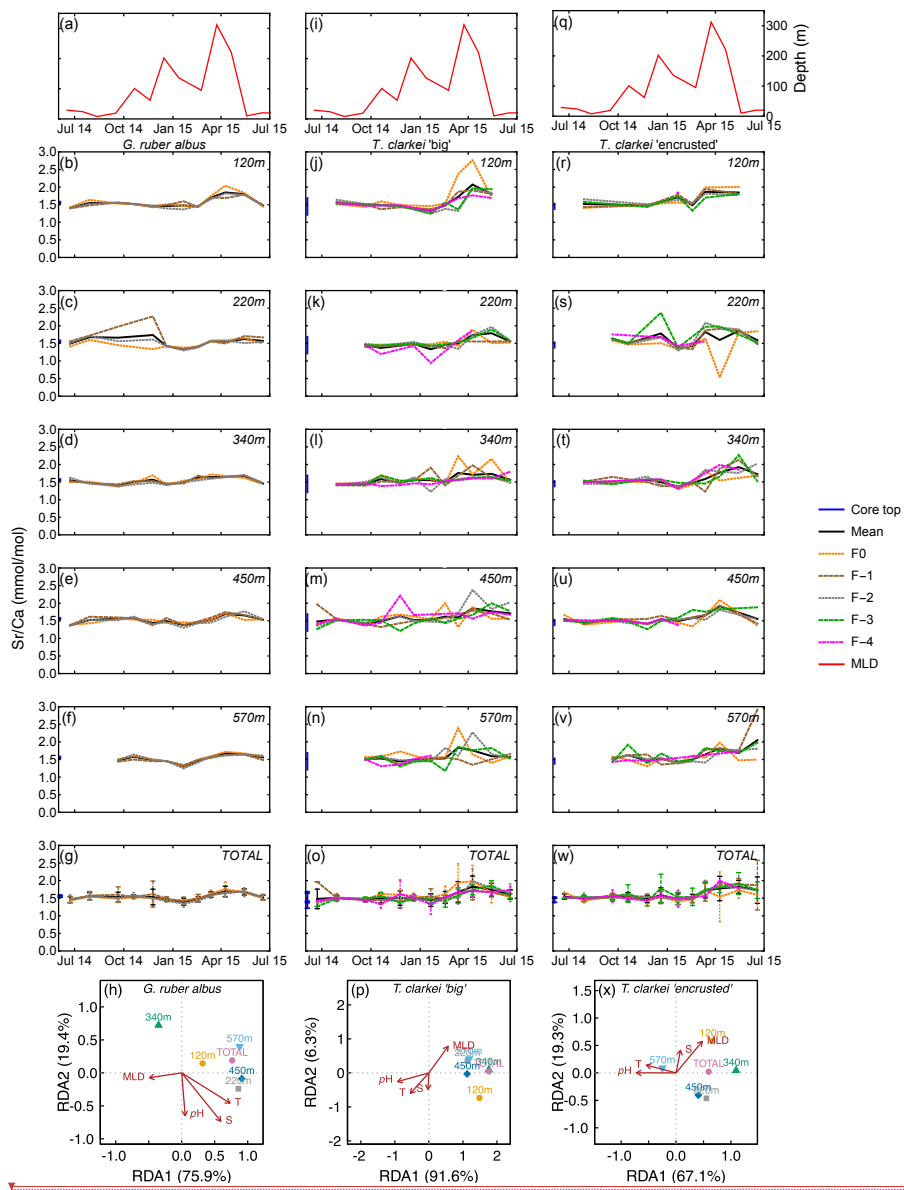
Deleted: 5o

Deleted: 5f

Deleted: 5o

Deleted: 5

Formatted: Font: Italic, Complex Script Font: Italic



382  
383 Figure 4: Time series of Sr/Ca values measured from the shells of *G. ruber albus* (b-f), *T.*  
384 *clarkei* 'big' (j-n) and *T. clarkei* 'encrusted' (r-v), derived from sediment traps located at  
385 different water depths (120-570 m). Sr/Ca of core top are marked by a blue bar along the left  
386 y-axes. Top panels a, i, and q show the depth (meters below surface layer) of the mixed layer

Deleted: 5

389 depth (MLD). Panels g, o, and w represent the average values of all depths for each chamber  
390 for each species. Panels h, p and x show the redundancy analysis (RDA) per species for each  
391 water depth with MLD depth, temperature, salinity and pH as explanatory variables. ▾

392 ▾  
393 B/Ca values range between 0.03 mmol/mol (570 m; January 2015) to 0.35 mmol/mol (120 m;  
394 June 2015) in *G. ruber albus*, with higher values during summer and spring and lower values  
395 during the winter (Figs. 5b to 5f). B/Ca measured in the final chamber, F0, are systematically  
396 lower compared to F-1 and F-2 values. Unlike most other element ratios, B/Ca values in both  
397 phenotypes of *T. clarkei* are similar to the range measured in *G. ruber albus*. In both *T. clarkei*  
398 phenotypes, lower B/Ca values were measured during the winter months, most prominently in  
399 January. The B/Ca values of *T. clarkei* 'big' range between 0.01 mmol/mol to 0.53 mmol/mol  
400 with some higher values during spring (Figs. 5k to 5n). B/Ca values in *T. clarkei* 'encrusted'  
401 range between 0.01 mmol/mol to 0.47 mmol/mol (Figs. 5r to 5v). Generally, B/Ca ICV is  
402 higher in *T. clarkei* than *G. ruber albus*, especially during spring (Figs. 5g, 5o, and 5w). The  
403 SD of *G. ruber albus* is highest at 0.086 during May 2015, at 120 m, and for *T. clarkei* 'big'  
404 and *T. clarkei* 'encrusted' the SD is 0.164 (450 m; June-July 2014) and 0.19 (120 m; May 2015)  
405 respectively. RDA analysis on B/Ca reveal a distinct RDA1 dominance in both *T. clarkei* 'big'  
406 and *T. clarkei* 'encrusted' (93.6% and 95.8%, respectively) compared to only 53.8% in *G. ruber*  
407 *albus*. In both *T. clarkei* phenotypes, the sediment trap data cluster together, showing a positive  
408 correlation with MLD and negative correlations with temperature, salinity, and pH. In contrast,  
409 *G. ruber albus* exhibits a more scattered distribution across water depths, with the 120 m and  
410 total samples showing a stronger alignment with MLD.

411

**Deleted:** Time series of Sr/Ca values measured from the shells of *G. ruber albus* (a-e), *T. clarkei* 'big' (f-j) and *T. clarkei* 'encrusted' (k-o), derived from sediment traps located at different water depths (120 m – 570 m).

**Deleted:** 4

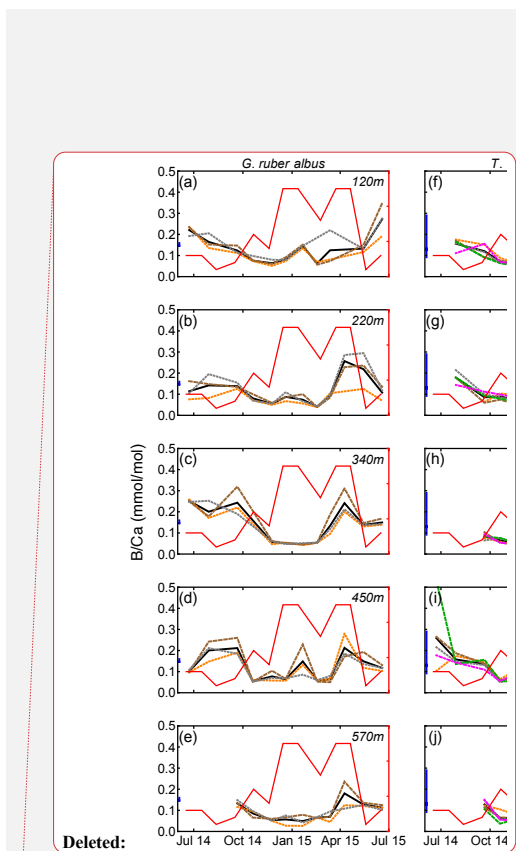
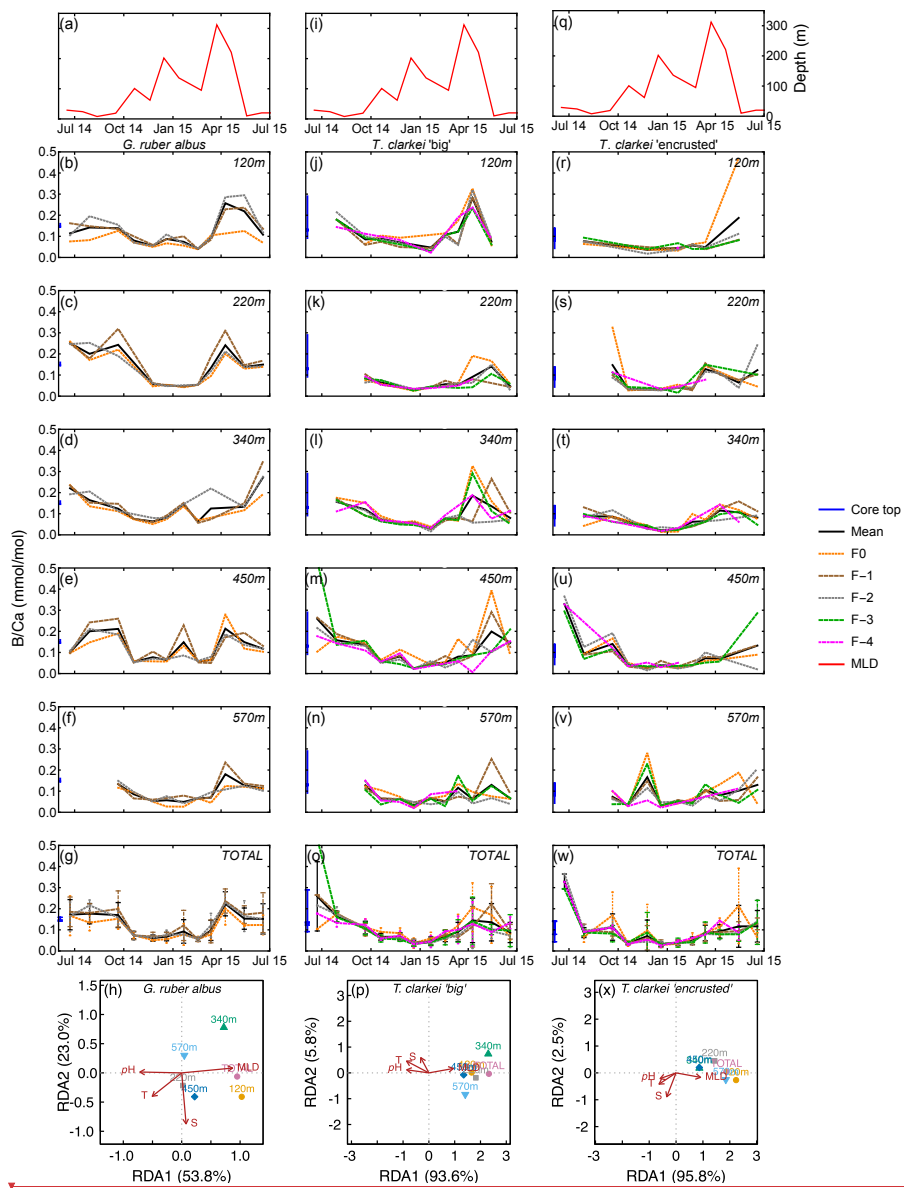
**Deleted:** 6a

**Deleted:** 6e

**Deleted:** 6f

**Deleted:** 6j

**Formatted:** Font: Italic, Complex Script Font: Italic



421

422 Figure 5: Time series of B/Ca values measured from the shells of *G. ruber albus* (b-f), *T. clarkei* 'big' (j-n) and *T. clarkei* 'encrusted' (r-v), derived from sediment traps located at different water depths (120-570 m). B/Ca of core top are marked by a blue bar along the left y-axes. Top panels a, i, and q show the depth (meters below surface layer) of the mixed layer depth (MLD).

423

424

425

428 Panels g, o, and w represent the average values of all depths for each chamber for each species.  
429 Panels h, p and x show the redundancy analysis (RDA) per species for each water depth with  
430 MLD depth, temperature, salinity and pH as explanatory variables.

431  
432 Na/Ca in *G. ruber albus* ranges between 6.60 mmol/mol (220 m; June-July 2014) to 64.14  
433 mmol/mol (220 m; April 2015) with a median value of 10.43 mmol/mol (Fig. 6; Fig. S1). The  
434 SD of Na/Ca ranges between 0.06 (570 m; February 2015) to 34.37 (120 m; April 2015). Na/Ca  
435 in *T. clarkei* 'big' ranges from 6.23 mmol/mol (570 m; September 2014) to 426.54 mmol/mol  
436 (220 m; March 2015) with a median value of 12.33 mmol/mol and SD range between 0.44 (570  
437 m; September 2014) to 106.33 (120 m; March 2015). Na/Ca in *T. clarkei* 'encrusted' ranges  
438 between 5.43 mmol/mol (570 m; September 2014) to 176.91 mmol/mol (570 m; March 2015)  
439 with a median value of 12.41 mmol/mol and SD reaches up to 64.64 (340 m; March 2015).  
440 *Globigerinoides ruber albus* has a low ICV during spring, while *T. clarkei* 'big' and 'encrusted'  
441 phenotypes display higher ICV during the same time interval. All morphotypes include  
442 significant excursions in Na/Ca with high values in *G. ruber albus* during January and April at  
443 220m (Fig. 6c), and high Na/Ca in both *T. clarkei* phenotypes at multiple depths and seasons  
444 (Figs. 6i-6m and 6p-6t). In particular, *T. clarkei* phenotypes show significant Na/Ca excursions  
445 during March-April and ICV (Figs. 6i-6t). RDA analysis on *T. clarkei* 'big' show, like B/Ca, a  
446 clustering of sediment trap data aligned with MLD and negatively correlated to pH, salinity  
447 and temperature positioned on the RDA1 axis (85.3%). The sediment trap data of *T. clarkei*  
448 'encrusted' show two distinct groups: 120 m, 220 m, 570 m and 'Total' together with MLD  
449 and the 350 m and the 450 m groups in the middle between MLD and pH, salinity and  
450 temperature, albeit slightly negative on the RDA2 axis (9.0%), while the explanatory  
451 parameters are positive on RDA2. The *G. ruber albus* Na/Ca displays a similar distribution to  
452 B/Ca however, the environmental parameters are aligned differently: MLD negative on RDA1  
453 axis (62.3%) and positive on RDA2 axis (28.1%); and, temperature, salinity and pH negative  
454 on RDA2 axis and positioned more to the center of RDA1. ▼

**Deleted:** Time series of B/Ca values measured from the shells of *G. ruber albus* (a-e), *T. clarkei* 'big' (f-j) and *T. clarkei* 'encrusted' (k-o), derived from sediment traps located at different traps from 120 m to 570 m water depths. ¶

**Deleted:** 7

**Deleted:** 7b

**Deleted:** 7f

**Deleted:** 7j

**Deleted:** 7k

**Deleted:** 7o

**Deleted:** 7f

**Deleted:** 7o

**Formatted:** Font: Italic, Complex Script Font: Italic

**Deleted:**

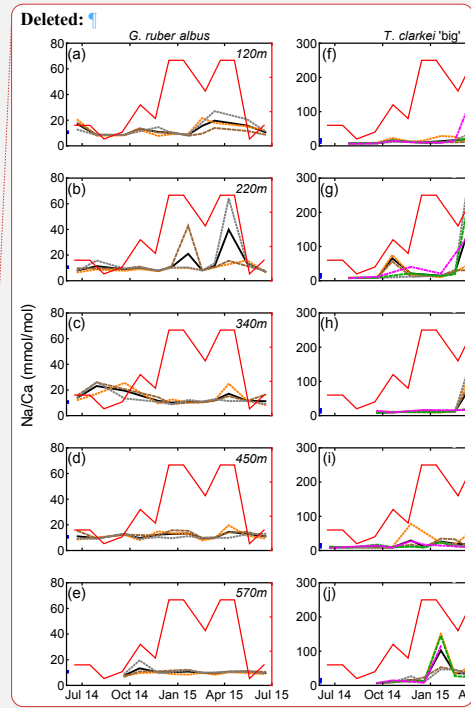
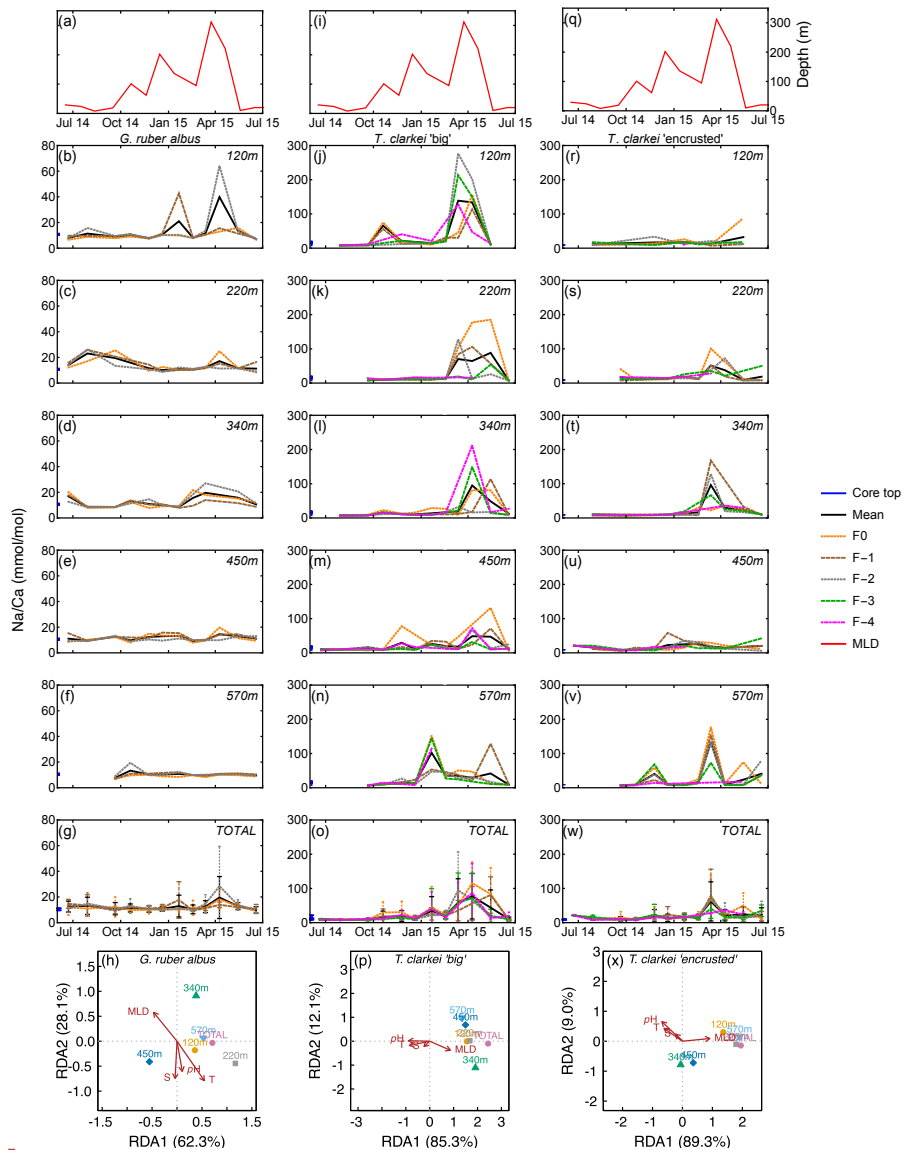


Figure 6: Time series of Na/Ca values measured from the shells of *G. ruber albus* (b-f), *T. clarkei* 'big' (j-n) and *T. clarkei* 'encrusted' (r-v), derived from sediment traps located at different water depths (120-570 m). Na/Ca of core top are marked by a blue bar along the left y-axes. Top panels a, i, and q show the depth (meters below surface layer) of the mixed layer depth (MLD). Panels g, o, and w represent the average values of all depths for each chamber

478 for each species. Panels h, p and x show the redundancy analysis (RDA) per species for each  
479 water depth with MLD depth, temperature, salinity and pH as explanatory variables. ▶

480  
481 Ba/Ca in *G. ruber albus* ranges from 0.73 µmol/mol (120 m; November 2014) to 36.81  
482 µmol/mol (340 m; June 2015). Ba/Ca in *T. clarkei* 'big' ranges from 0.39 µmol/mol (120 m;  
483 June 2015) to 246.54 µmol/mol (450 m; March 2015). Ba/Ca in *T. clarkei* 'encrusted' ranges  
484 from 0 µmol/mol (April 2015) to 171.41 µmol/mol (340 m; March 2015) (Fig. 7; Fig. S1). The  
485 three morphotypes display varied ICV, although *T. clarkei* shows more prominent ICV during  
486 spring months with SD values of 42.06 (340 m; April 2015, 'encrusted') and 98.98 (450 m;  
487 March 2015, 'big') (Figs. 7i-7t and supplementary table S4) than *G. ruber albus* with SD values  
488 of 19.14 (220 m; June-July 2014) (Figs. 7b-7f). Furthermore, RDA analyses exhibit for both *T.*  
489 *clarkei* phenotypes, a clear RDA1 dominance with 93.6% and 95.8% for 'big' and 'encrusted'  
490 respectively. Additionally, for both types, sediment trap data is clustered with positive  
491 correlation to MLD and negative to temperature, salinity and pH. For *G. ruber albus*, RDA1  
492 value is 53.8% and RDA2 is 23.0%. The sediment traps data are scattered and while the  
493 environmental parameters temperature and salinity point together negatively on the RDA2 axis,  
494 MLD and pH are positioned on opposite directions on the RDA1 axis (positive and negative  
495 respectively).

**Deleted:** Time series of Na/Ca values measured from the shells of *G. ruber albus* (a-e), *T. clarkei* 'big' (f-j) and *T. clarkei* 'encrusted' (k-o), derived from sediment traps located at different water depths (120 m – 570 m). ¶

**Deleted:** 8

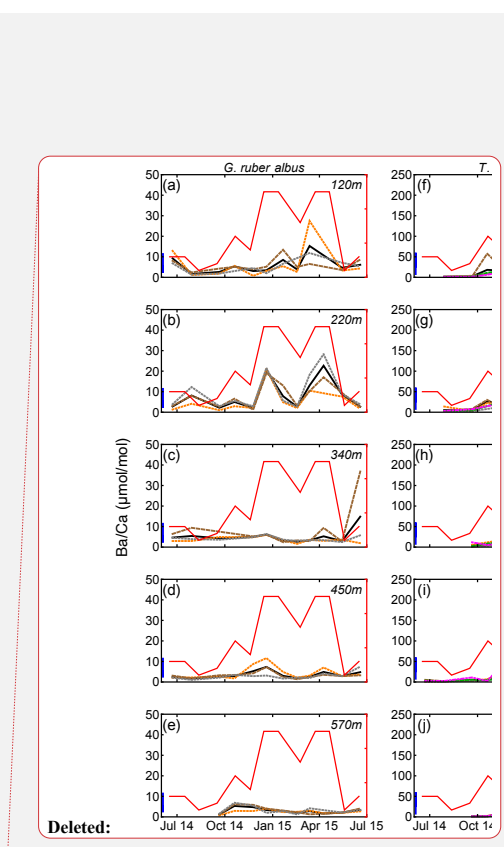
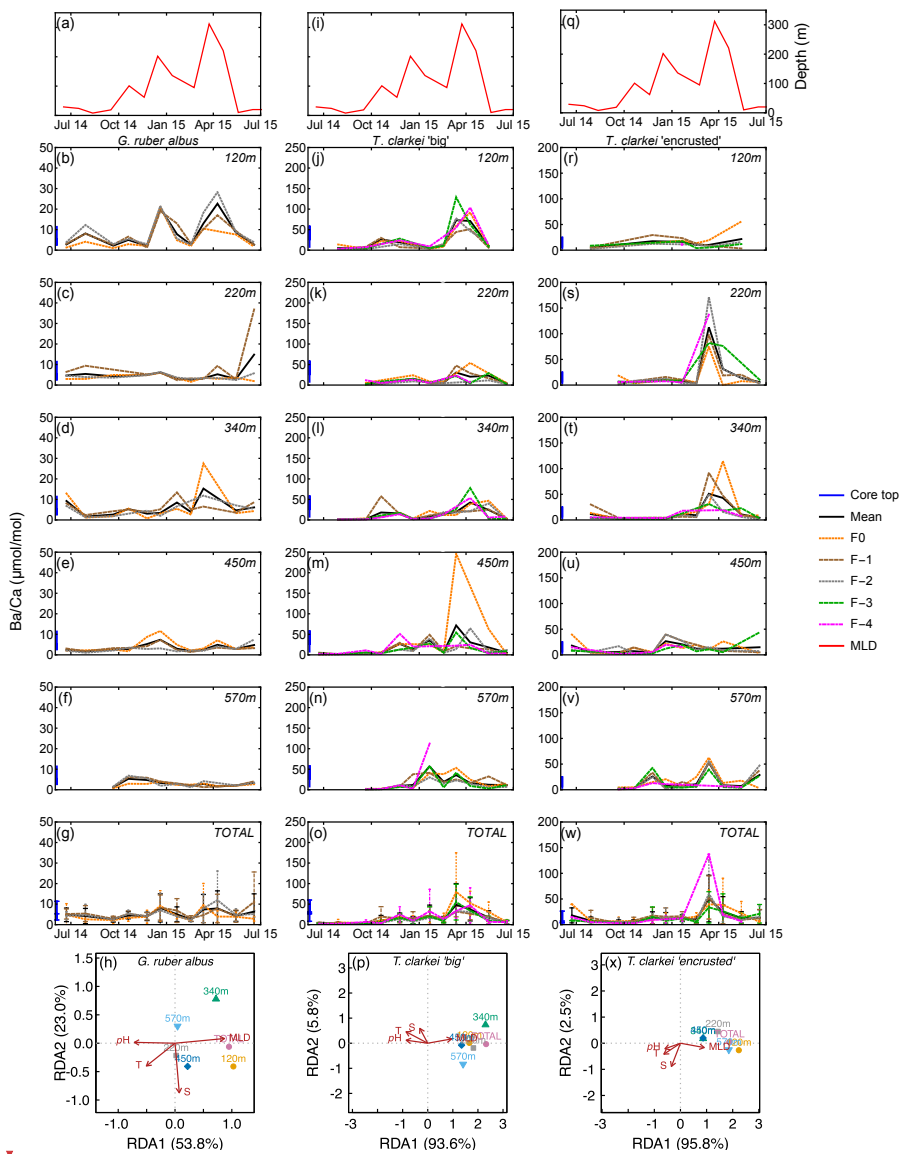
**Deleted:** 8f

**Deleted:** 8o

**Deleted:** 8a

**Deleted:** 8e

**Formatted:** Font: Italic, Complex Script Font: Italic



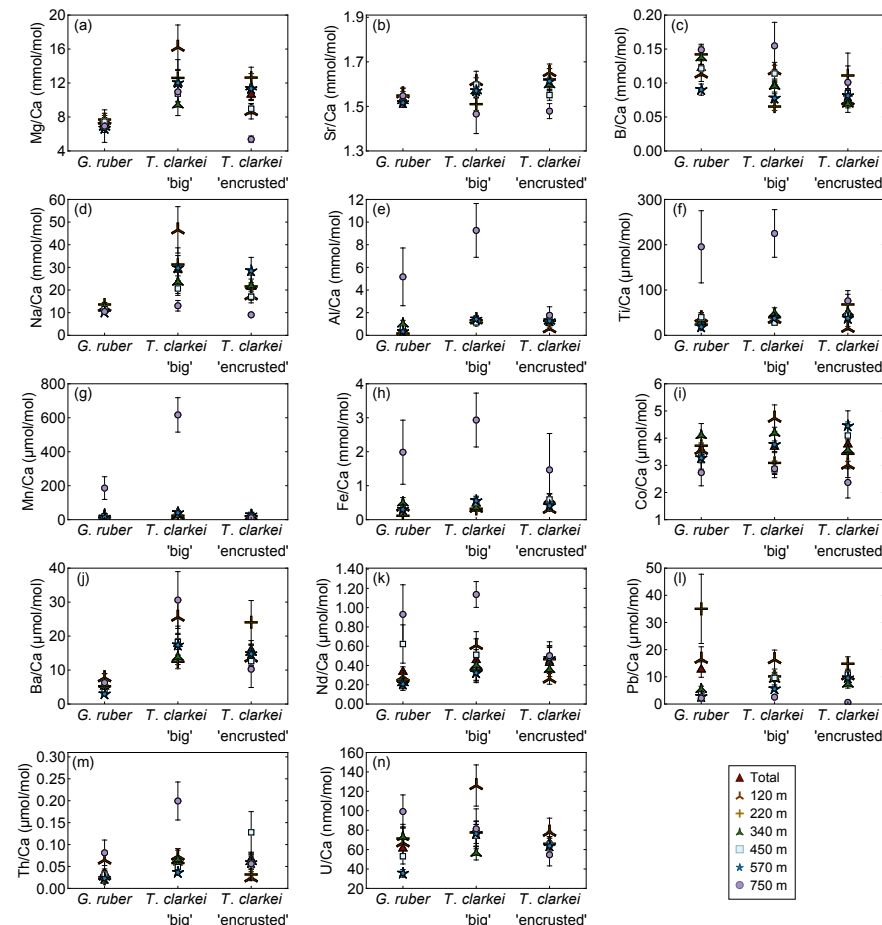
Deleted: 8

505  
506 Figure 7: Time series of Ba/Ca values measured from the shells of *G. ruber albus* (b-f), *T.*  
507 *clarkei* 'big' (j-n) and *T. clarkei* 'encrusted' (r-v), derived from sediment traps located at  
508 different water depths (120-570 m). Ba/Ca of core top are marked by a blue bar along the left  
509 y-axes. Top panels a, i, and q show the depth (meters below surface layer) of the mixed layer  
510 depth (MLD). Panels g, o, and w represent the average values of all depths for each chamber

513 for each species. Panels h, p and x show the redundancy analysis (RDA) per species for each  
 514 water depth with MLD depth, temperature, salinity and pH as explanatory variables.

### 516 3.2. Depth-averaged values of element/Ca measured in *G. ruber albus* and *T. clarkei* shells 517 using LA-ICP-MS

518 Generally, the means of Mg/Ca, Sr/Ca, B/Ca, Na/Ca and Ba/Ca in *G. ruber albus* indicate that  
 519 the composition of tests, from most water depths is similar to that of core-top samples (Figs.  
 520 8a-8d, 8j). In contrast, Al/Ca, Ti/Ca, Mn/Ca, Fe/Ca, Nd/Ca, Th/Ca, and U/Ca (Figs. 8e-8i, 8k,  
 521 8m, 8n) in the tests from sediment interface were higher than in the water column, and lower  
 522 in case of Co/Ca and Pb/Ca (Figs. 8i, 8l).



**Deleted:** Time series of Ba/Ca values measured from the shells of *G. ruber albus* (a-e), *T. clarkei* 'big' (f-j) and *T. clarkei* 'encrusted' (k-o), derived from sediment traps located at different water depths (120 m – 570 m). ¶

**Formatted:** Font colour: Text 1

**Formatted:** Justified, Indent: Before: 0.75 cm, Hanging: 0.5 cm

**Deleted:** ¶

**Deleted:** 3

</div

539 Figure 8: Pooled mean values of the calcium-normalized element ratios of *G. ruber albus*, *T.*

540 *clarkei* ‘big’ and *T. clarkei* ‘encrusted’ shells, derived from sediment traps located at different

541 water depths (120 m to 570 m) and a core top sample (750 m) from the Gulf of Aqaba. Error

542 bars represent 1 sigma relative standard error ( $SD/\sqrt{n}$ )

543

544 Furthermore, *T. clarkei* tends to demonstrate higher values and higher variability compared to

545 *G. ruber albus* (e.g., Mg/Ca, Na/Ca, Ba/Ca, Nd/Ca). Compared to the core-top samples, *T.*

546 *clarkei* from the water column also exhibit relative enrichment in Al/Ca, Ti/Ca, Mn/Ca, Fe/Ca,

547 Nd/Ca, B/Ca, and Th/Ca (*T. clarkei* ‘big’), and depletion in Co/Ca, Pb/Ca, Sr/Ca, and Mg/Ca

548 (*T. clarkei* ‘encrusted’) (Fig. 8).

549

### 550 3.3 Relationships between element/Ca and environmental parameters.

551 A Spearman correlation matrix was applied to assess the relationships of the element/Ca and

552 environmental variables in the three analyzed PF phenotypes (Fig. 9; Tab. S2; Fig S12). The *T.*

553 *clarkei* types exhibit similar pattern of relationships, with minor differences mainly in

554 correlation strength (Fig. 9a, 9b). In general, *T. clarkei* shows more significant relationships

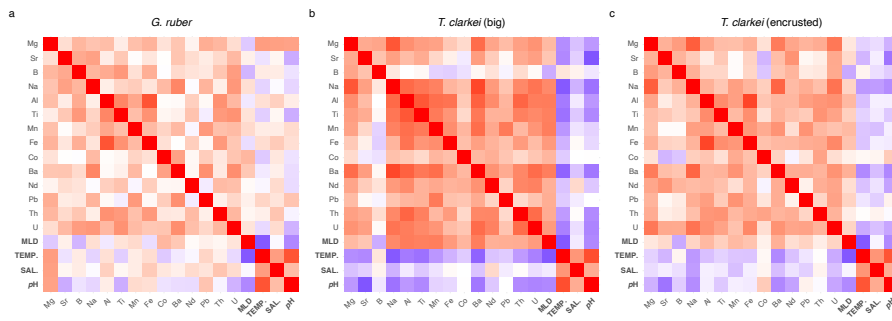
555 than *G. ruber albus*, while, *G. ruber albus*, display different relationships to those of the two

556 *T. clarkei* types. In *T. clarkei*, Mg/Ca displays relatively strong relationships with Na/Ca,

557 Ba/Ca, and Al/Ca (Fig. 9b, 9c). Sr/Ca, B/Ca, Co/Ca and Nd/Ca do not display significant

558 relationships to other elements in *G. ruber albus* as well as in *T. clarkei* ‘big’ and *T. clarkei*

559 ‘encrusted’.



560

561 Figure 9: Spearman correlation Matrix of element-Ca means in *G. ruber albus* (a), *T. clarkei* ‘big’ (b) and, *T. clarkei* ‘encrusted’ (c) and environmental variables.

Deleted: 3

Formatted: Not Highlight

Deleted: 3

Deleted: of the different PF species in the GOA

Formatted: Font colour: Text 1

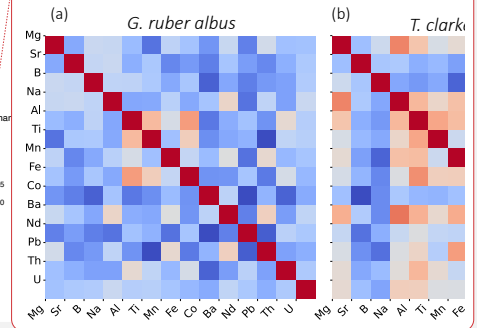
Formatted: Font colour: Text 1

Formatted: Normal, Indent: Before: 0.63 cm, Hanging: 0.62 cm, No bullets or numbering

Deleted: numerical

Deleted: ¶

Deleted:



Deleted: the different trace

Deleted:

Deleted: normalized abundances

Formatted: Justified

Deleted: ¶

574 For both *T. clarkei* 'big' and *T. clarkei* 'encrusted', Na/Ca significantly correlates with  
575 Al/Ca, Mn/Ca, and Ba/Ca, the later showing the strongest relationships in *T. clarkei* 'big' ( $r =$   
576 0.82, Fig. 9b; Tab. S2). Relationships between Al/Ca, Ti/Ca, Mn/Ca, Fe/Ca, Ba/Ca and Th/Ca  
577 are generally stronger in *T. clarkei* 'big' than in *T. clarkei* 'encrusted', except for Al/Ca and  
578 Fe/Ca, which are stronger related in *T. clarkei* 'encrusted' ( $r = 0.85$ ; Tab. S2) than in *T. clarkei*  
579 'big' ( $r = 0.74$ ; Tab. S2). Unlike *G. ruber albus*, the U/Ca in *T. clarkei* exhibit relatively strong  
580 relationships with Ba/Ca, Na/Ca and Al/Ca (in *T. clarkei* 'big') and Mg/Ca (in *T. clarkei*  
581 'encrusted', Fig. 9c) while in *G. ruber albus*, U/Ca is poorly related to the other elements (Fig.  
582 9a). Mg/Ca of *G. ruber albus*, has a positive correlation with temperature, salinity, and pH, and  
583 a negative correlation with MLD; other element/Ca in *G. ruber albus* do not exhibit significant  
584 correlations with these environmental variables (Fig. 9a). By contrast, in *T. clarkei* ('big' and  
585 'encrusted'), element/Ca show strong correlations with MLD but not with T temperature,  
586 salinity, or pH (Figs. 9b, 9c). In the *T. clarkei* 'big' morphotype, SD (ICV) shows strong  
587 correlations between multiple element/Ca and with MLD. On the other hand, in *T. clarkei*  
588 'encrusted' and *G. ruber albus*, correlations are weaker and/or inconsistent across variables,  
589 and no uniform pattern emerges.

590

#### 591 4. Interpretation

##### 592 4.1 Inter chamber variability (ICV)

593 Shell-bound element/Ca display varying trends across different chambers depending on the  
594 specific element ratios, and varying over water depth and time (Figs. 3-7). In most element/Ca  
595 ICV is higher during water column mixing months (March-May; e.g., Al/Ca, B/Ca, Ba/Ca,  
596 Co/Ca, Fe/Ca, Mg/Ca) in all water depth horizons for *T. clarkei* 'big' and *T. clarkei* 'encrusted',  
597 while for *G. ruber albus* it increases in the two upper water depth horizons (i.e., 120 m and 220  
598 m). Elevated element/Ca values and high ICV may reflect the changes in the water properties  
599 like the temperature, salinity, pH and nutrient availability derived from the mixing of the water  
600 column (Fig. S12, Figs 3-7 panels h, p, and x). For some element/Ca ratios (e.g., Na/Ca, Fig.  
601 6/panels g, o, and w; Ba/Ca, Fig. 7/panels g, o, and w) ICV varies with depth and shows  
602 seasonal differences (i.e., less variation with depth during water column stratification and more  
603 variation with depth during water column mixing), whereas for others (e.g., B/Ca, Fig. 5/panels  
604 g, o, and w; Sr/Ca, Fig. 4/panels g, o, and w) it remains relatively constant with depth. In the  
605 *T. clarkei* 'big' morphotype, ICV shows strong correlations across most element/Ca and with  
606 MLD, indicating that increases in ICV reflects a common driver, most likely the mixed-layer  
607 depth (Fig. S12).

Formatted: Font: Italic, Complex Script Font: Italic

Formatted: Font: Italic, Complex Script Font: Italic

Formatted: Font: Not Italic, Complex Script Font: Not Italic

Formatted: Font colour: Text 1

Formatted: Outline numbered + Level: 1 + Numbering Style: 1, 2, 3, ... + Start at: 1 + Alignment: Left + Aligned at: 0.63 cm + Indent at: 1.27 cm

Deleted: 4

Deleted: 8

Formatted: Font: Italic, Complex Script Font: Italic

Formatted: Font: Italic, Complex Script Font: Italic

Formatted: Font: Italic, Complex Script Font: Italic

610 Typically, most PF reproduction-cycles span about a month with individual chambers forming  
611 within several hours (Bé et al., 1977), while the time interval between chamber formation can  
612 range from hours to weeks (Schiebel & Hemleben, 2017, and references therein). Setting aside  
613 the March-May time-interval where PF shells show exceptionally high ICV, *G. ruber albus*  
614 generally exhibits lower values (e.g., Mg/Ca, B/Ca), and less ICV compared (e.g., Mg/Ca  
615 SD=1.67) to *T. clarkei* 'big' and 'encrusted' (e.g., Mg/Ca SD=5.24 for 'big' type and Mg/Ca  
616 SD=3.55 for 'encrusted' type). The residence of *G. ruber albus* in the relatively homogenous  
617 and narrow living environment in the surface mixed layer (Schiebel & Hemleben, 2017;  
618 Thirumalai et al., 2014; and others), could explain relatively lower ICV. In contrast, *T. clarkei*  
619 dwell in the dynamic region near/under the thermocline (Schiebel & Hemleben, 2017; Levy et  
620 al., 2023) over a wider dwelling depth horizon, and may experience more heterogeneous  
621 environmental conditions which may result in higher ICV.

622 The secondary crust observed on *T. clarkei* 'encrusted' morphotypes, which covers all  
623 chambers of the tests analyzed here, does not significantly alter element/Ca values when  
624 compared to *T. clarkei* 'big', unlike the crust of *Neogloboquadrina dutertrei* (Jonkers et al.,  
625 Nonetheless, the RDA (Figs. 3-7) and the Spearman correlation analyses (Fig. 9) of both  
626 *T. clarkei* types indicate that while *T. clarkei* 'big' show a positive correlation to MLD and a  
627 weaker or negative correlation to other environmental parameters (T, S and pH), the *T. clarkei*  
628 'encrusted' type calcification mechanism is more complex and could be influenced by  
629 additional factors / environmental variables. Therefore, while both types are eligible for  
630 paleoceanography and paleoclimate reconstructions, the interpretation of their measurements  
631 might be different.

632 The ultimate chamber (F0) presents different systematics compared to the preceding  
633 chambers in both *T. clarkei* and *G. ruber albus* (Fig. S11). In *T. clarkei* (both 'big' and  
634 'encrusted'), the F0 typically exhibits higher values of B/Ca, Na/Ca, Mg/Ca, and Al/Ca  
635 compared to the previous chambers. In contrast, *G. ruber albus* displays relatively lower values  
636 in F0 for the same ratios highlighting species-specific differences in chamber formation (Fig.  
637 S11). Interestingly, Sr/Ca does not follow the same pattern. In *T. clarkei* 'big' the Sr/Ca  
638 distribution mirrors the trends of other elements, while F0 in *G. ruber albus* and *T. clarkei*  
639 'encrusted' shows an even distribution of Sr/Ca, likely reflecting the relatively constant Sr/Ca  
640 values in the water column during the lifespan of a single test. These observations in *G. ruber*  
641 *albus* are consistent with previous studies that measured Mg/Ca in individual chambers (Bolton  
642 et al., 2011; Davis et al., 2020; Fischer et al., 2024). The contrasting systematics of F0 leading  
643 to elevated ICV in the ultimate chamber compared to the previous chambers was previously

**Deleted:** April

**Formatted:** Not Highlight

**Deleted:** analysed

**Formatted:** Font: Italic, Complex Script Font: Italic

**Formatted:** Not Highlight

**Deleted:** This suggests that the secondary calcite layer in *T. clarkei* 'encrusted' does not play a major role in element incorporation or ICV and is affected by the same mechanisms which control the formation of the ontogenetic calcite, and thus would facilitate application of our finding to the interpretation of fossil *T. clarkei* 'encrusted' in paleoceanography and paleoclimate reconstructions.

653 suggested to be associated with a chamber wall that is not fully calcified (Schiebel &  
654 Hemleben, 2017; Bolton et al., 2011; Fischer et al., 2024). Differences in F0 systematics  
655 between *T. clarkei* and *G. ruber albus* could be driven by species-specific calcification  
656 processes, though further research is needed to clarify this issue. Additionally, it is important  
657 to consider potential biases in small chambers such as F-4 in *T. clarkei* morpho-species, where  
658 methodological challenges (e.g., laser spots hitting sutures) may skew element/Ca  
659 measurements. Consequently, we conclude that the exclusion of F0 and F-4 ~~may~~ enhance the  
660 ~~robustness~~ of reconstructions of the marine environment in studies of downcore records.  
661

Deleted:

Deleted: will

Deleted: reliability

#### 662 4.2 Relationships of element ratios of the three PF morphotypes

663 The contrasting results of the correlation matrixes of the three morpho-species, suggests  
664 species-specific mechanisms while calcifying their shells. The Mg/Ca in *T. clarkei* which  
665 strongly correlates with Na/Ca, Ba/Ca, and Al/Ca (Fig. 9b, 9c), suggests more than one  
666 environmental process affects Mg/Ca in the tests as the other element/Ca are considered proxies  
667 to different environmental characteristics such as salinity, productivity, and terrigenous input  
668 (Chang et al., 2015; Mesa-Fernández et al., 2022; Beasley, et al., 2021). This is also reinforced  
669 by the positive correlation to MLD and the negative correlation to temperature, salinity and pH  
670 (Fig. 9 and RDA panels in figs. 3-7). Additionally, Mg/Ca in *G. ruber albus* show a relative  
671 strong positive correlation to temperature, salinity and pH and a negative correlation to MLD  
672 (Fig. 9a and Figs. 3h, 3p and 3x). Similar to *G. ruber albus*, in the *T. clarkei* types Sr/Ca, B/Ca,  
673 Co/Ca and Nd/Ca display a much weaker relationship to other elements making them more  
674 suitable proxies for distinct and independent environmental properties.

Formatted: Font: Italic, Complex Script Font: Italic

Formatted: Font: Italic, Complex Script Font: Italic

Formatted: Font: Italic, Complex Script Font: Italic

675 In *G. ruber albus*, Mg/Ca, Sr/Ca and B/Ca show no significant relationships with other element  
676 ratios, indicating that independent processes likely govern their proxy systematics (Fig. 9c).  
677 Similarly, Co/Ca, Nd/Ca and U/Ca also do not correlate with other element/Ca. While Na/Ca  
678 and Ba/Ca exhibit some degree of correlation, as do Mn/Ca and Pb/Ca, the lithophilic elements,  
679 Al/Ca, Ti/Ca, which are considered proxies for terrigenous dust input (Chang et al., 2015;  
680 Mesa-Fernández et al., 2022; Beasley, et al., 2021), as well as, Fe/Ca, and Th/Ca, all show a  
681 relative strong correlation. Their correlation implies they can be used together for  
682 reconstructing terrigenous input to the water column. Among the lithophilic elements, Th/Ca  
683 display a relatively weaker relationship, suggesting a potential effect of additional processes  
684 such as scavenging (Anderson et al., 1983; Francois et al., 2004; Costa et al., 2020).

Deleted: do not display statistically significant relationships

685

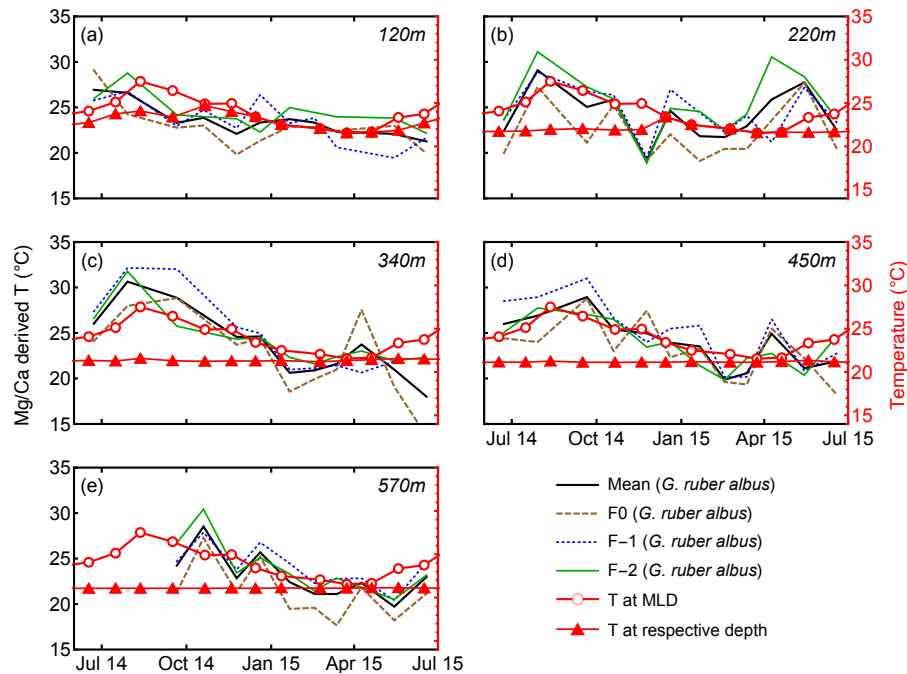
#### 686 4.3 Mg/Ca as a proxy for sea surface temperature

691 Shell-bound Mg/Ca of calcareous foraminifera have been extensively utilized as a paleo-  
692 thermometer (e.g., Nürnberg et al., 1996; Sadekov et al., 2009). Many of these Mg-temperature  
693 calibrations rely on whole-test or pooled-mean Mg/Ca values to reconstruct past sea surface  
694 temperatures (Spero et al., 2003; Ganssen et al., 2010; and others). Several studies have  
695 measured intra-test and inter-test Mg/Ca in an effort to produce Mg-temperature calibrations  
696 using single chamber measurements of *G. ruber* (Sadekov et al., 2008; Bolton et al., 2011;  
697 Davis et al., 2020; Levy et al., 2023; Fischer et al., 2024). Previous work on sediment trap-  
698 derived specimens of *T. clarkei* and *G. ruber albus* from the GOA indicated that *T. clarkei* is  
699 not suitable for temperature reconstructions, due to its presumed deep dwelling-depth below  
700 the thermocline together with its high sensitivity to water column mixing events. However,  
701 while *G. ruber albus* shows exceptionally high pooled mean Mg/Ca values in the GOA in  
702 comparison to other ocean regions, it also exhibits seasonal variations that indicate effective  
703 applicability as a paleothermometer (Levy et al., 2023). Due to the high seawater salinity of  
704 the GOA, a local calibration curve was proposed (Eq. 1; Levy et al., 2023).

705

706 
$$\frac{\text{Mg}}{\text{Ca}} = 0.39(\pm 0.30) \cdot e^{0.12(\pm 0.03)T} \quad (1)$$

707



708

709 Figure 10: *G. ruber albus* Mg/Ca-derived temperatures versus measured temperatures (red).  
 710 The calculated temperatures were derived from Eq. 1 for individual chambers. See also Levy  
 711 et al. (2023).

712

713 Pooled mean values of Mg/Ca in *G. ruber albus* taken from all water column depths in the  
 714 GOA reflect MLD temperatures (Fig. 10, Fig. 9). Inter-chamber variability (ICV) has been  
 715 shown to affect the local Mg/Ca temperature calibration (Eq. 1) of *G. ruber albus* (Levy et al.,  
 716 2023; Fig. 10). Generally, Mg/Ca-derived temperatures from chambers F-1 and F-2 correspond  
 717 closely with mixed layer depth (MLD) temperatures. However, beneath the photic zone, Mg/Ca  
 718 of all three chambers F0, F-1, and F-2 of the *G. ruber albus* specimens exhibit poor fits with  
 719 measured temperatures (Fig. 10). Given that *G. ruber albus* calcifies its shell in the photic zone  
 720 (Schiebel and Hemleben, 2017), these findings support the use of Mg/Ca as a  
 721 paleothermometer for the mixed layer (Nürnberg et al., 1996). Sadekov et al. (2009) measured  
 722 F0-Mg/Ca in core top individuals of *G. ruber albus* from various latitudes and have reported  
 723 an agreement with sea surface temperature. Hupp and Fehrenbacher (2024) measured intra-test  
 724 variability in the polar and sub-polar species *Neogloboquadrina incompta*, *N. pachyderma*, and  
 725 *Turborotalita quinqueloba* and have not reported any issues regarding the use of F0 for

Moved (insertion) [1]

Formatted: Not Highlight

Formatted: Font: Italic, Complex Script Font: Italic

726 temperature reconstruction. In the GOA however, the Mg/Ca-derived temperatures from  
727 chamber F0 calculate lower Mg/Ca temperatures of the MLD than chambers F-1 and F-2 (Fig.  
728 10). Although Mg/Ca data from chambers F-1 and F-2 appear suitable for reconstructing  
729 temperatures and demonstrate agreement with MLD temperature trends, the high ICV in *G.*  
730 *ruber albus* is evidently too great to accurately reflect ambient temperatures using this  
731 calibration. Therefore, and based on these new observations, we suggest that optimal Mg/Ca-  
732 temperature calibration (Eq. 1) should be based on the pooled mean of the F-1 and F-2  
733 chambers at all depths as the final chamber might lead to different results while reconstructing  
734 temperature.

735

#### 736 4.4 B/Ca as a proxy for pH

737 B/Ca in some PF species has been suggested to be a proxy for pH (Yu et al., 2007; Allen et al.,  
738 2011). Comparing chamber B/Ca of both *G. ruber albus* and *T. clarkei* (both ‘big’ and  
739 ‘encrusted’) alongside pH at various water column depths in the GOA reveals contrasting  
740 results. While B/Ca in *G. ruber albus* exhibits seasonality (Fig. 5), with lower values during  
741 winter months, it does not appear to be consistent with the pH of respective water depth nor  
742 the MLD (Fig. 11). This inconsistency suggests that B/Ca in *G. ruber albus* from the GOA is  
743 not a reliable recorder of ambient water pH. Similarly, Henehan et al. (2015) and Naik & Naidu  
744 (2014) reported that B/Ca of open ocean core-top samples and down-core sediment samples do  
745 not display a pH relationship.

746 Alternatively, B/Ca in *G. ruber albus* may be sensitive to salinity and micro-environments  
747 produced by PF symbionts with pH levels which are distinct from the ambient water column.  
748 Culture experiments have shown that B/Ca is affected by salinity and increases with increasing  
749 salinity (Allen et al., 2012). However, only small salinity changes occur in the GOA (Fig. 1),  
750 which argue against a strong B/Ca-salinity relationship that would result in a B/Ca seasonal  
751 trend. It was suggested that photo-symbionts such as dinoflagellates in *G. ruber albus* create  
752 micro-environments with pH levels, which are distinct from ambient seawater, to accommodate  
753 for their photosynthetic activity, and indicate that B/Ca is more affected by pH in those micro-  
754 environments than the water column pH (Hönisch et al., 2021; Babila et al., 2014). An  
755 additional observation for the *G. ruber albus* B/Ca values is that they are relatively high in  
756 comparison to values from other studies. The relatively high salinity in the GOA (~41),  
757 combined with the photosymbiont activity in *G. ruber albus* may explain the elevated B/Ca  
758 values (Henehan et al., 2015; Hönisch et al., 2021; Babila et al., 2014).

Deleted: T

Deleted: show

Deleted: .

Formatted: Font colour: Text 1

Formatted: Outline numbered + Level: 2 + Numbering Style: 1, 2, 3, ... + Start at: 4 + Alignment: Left + Aligned at: 0.63 cm + Indent at: 1.27 cm

Deleted: 6

Deleted: s

764 In contrast to *G. ruber albus*, B/Ca in the photosymbiont barren *T. clarkei* may possibly record  
 765 the changes in pH (Fig. 11) of seawater at its assumed ambient dwelling depth (i.e., 340 m-570  
 766 m), indicative of shifting between the deeper water column depth horizons where pH changes  
 767 are evident. Based on the fluxes of *T. clarkei* (Chernihovsky et al., 2018; Fig. 2), the B/Ca of  
 768 *T. clarkei* in the sediment record likely represent the pH beneath the thermocline and within  
 769 the deep-water column horizons for specimens that lived from early winter through spring. In  
 770 particular, pH at 340 m trends appear to follow the B/Ca trends of *T. clarkei* types. For B/Ca-  
 771 pH calibrations utilizing the pooled mean of data from the chambers F-1, F-2, and F-3 may be  
 772 used, while excluding the F0 and F-4 chambers where more ICV is visually apparent (Fig. 11).  
 773

**Deleted:** indeed

**Deleted:** possibly

**Deleted:** Indeed, b

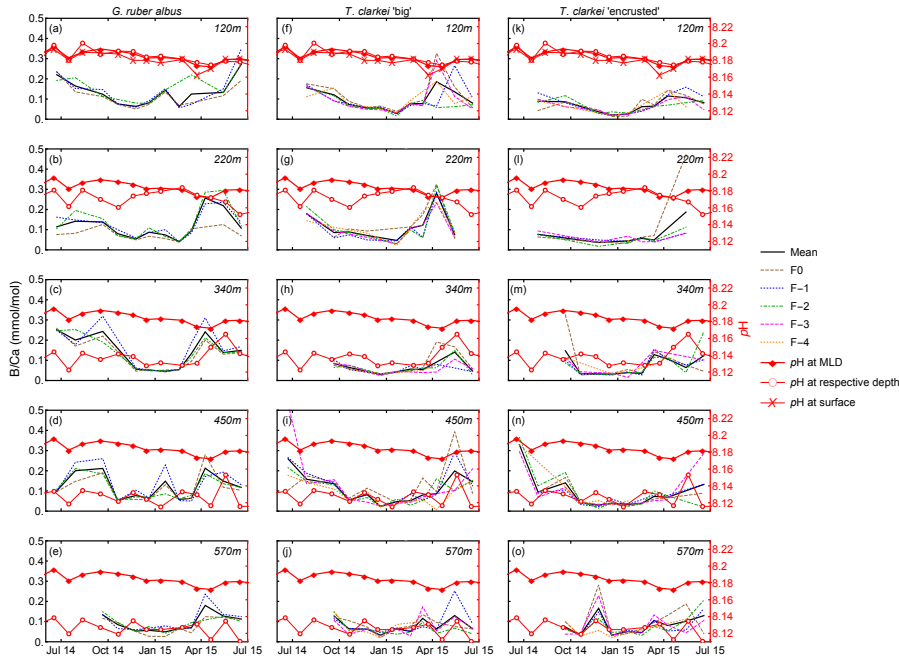
**Deleted:** s

**Deleted:** correlate

**Deleted:** with

**Deleted:** is recommended

**Deleted:** ICV



774  
 775 Figure 11: Single chamber B/Ca and in situ pH measured at MLD depth (empty red circles)  
 776 and 120 m water depth for *G. ruber albus*, *T. clarkei* 'big' and *T. clarkei* 'encrusted'.  
 777

778 4.5 Na/Ca as a proxy for salinity and Ba/Ca as an indicator for productivity

779 Cultured individuals and samples from the surface Caribbean and the Gulf of Guinea of live *T.*  
 780 *sacculifer* indicate that Na/Ca can be used as a proxy for salinity, without temperature  
 781 dependence, however, a species-specific calibration might be required (Bertlich et al., 2018).

**Formatted:** Indent: Hanging: 0.77 cm, Outline numbered +  
 Level: 2 + Numbering Style: 1, 2, 3, ... + Start at: 4 +  
 Alignment: Left + Aligned at: 0.63 cm + Indent at: 1.27 cm

790 Despite the high variability of PF Na/Ca values in the GOA during water column mixing (Fig.  
791 6), salinity remains high and relatively constant, ranging between 40.4-40.7. Consequently, a  
792 local Na/Ca-salinity calibration shows no significant relationship for any of the three PF  
793 morphotypes.

Deleted: 7

794 Na/Ca values in PF from the GOA are notably higher compared to other regions. Gray *et*  
795 *al.* (2023) explored the relationship between Na/Ca and salinity in *G. ruber albus* collected  
796 from sediment traps, plankton tows, culture samples, and core top samples, contributing to the  
797 ongoing discussions regarding the reliability of Na/Ca as a proxy for salinity in both planktic  
798 and benthic foraminifera (Allen *et al.*, 2016; Geerken *et al.*, 2018; Mezger *et al.*, 2016, 2018;  
799 Gray *et al.*, 2023, and references therein). They concluded that the measurement method (i.e.,  
800 ‘solution’ ICP-MS vs. LA-ICP-MS) influences the values of Na/Ca and in turn the relationship  
801 with salinity, i.e., weak in solution-based compared to significant in laser ablation-based, at  
802 salinity over 36.

803 Comparing Na/Ca of *G. ruber albus* from the shallowest sediment trap (120 m) in the GOA  
804 with the Na/Ca of *G. ruber albus* plankton tows-samples from the GOA deployed and collected  
805 in January 2010 and October 2013 (Gray *et al.*, 2023), both measured using LA-ICP-MS,  
806 generally reveals similar results, excluding the high-value excursions observed in some single  
807 chamber measurements (Fig. 6). *Turborotalita clarkei* in the GOA exhibits elevated Na/Ca  
808 values in both ‘big’ and ‘encrusted’ compared to *G. ruber albus*. Unlike *G. ruber albus*, there  
809 is relatively higher variability between water depths as well as significantly higher values in  
810 March, April, and May associated with water column mixing (Fig. 6). During these mixing  
811 events, nutrient-rich, high salinity (~40.7) water ascend upward. Therefore, the Na/Ca of *T.*  
812 *clarkei* may serve as a proxy for water column stability, i.e., stratification vs. mixing.

Deleted: 7

813 The Ba/Ca in the three morpho-species show a relatively strong correlation with Na/Ca  
814 (0.74 and 0.82 in *T. clarkei* ‘big’ and ‘encrusted’ respectively, and 0.54 in *G. ruber albus*, the  
815 second highest ratio and exceeded only by the 0.57 of Pb/Ca). Ba/Ca is presumably unaffected  
816 by temperature, salinity, and pH (Hönisch *et al.*, 2011). In non-spinose species, Ba/Ca typically  
817 shows positive relationships with productivity and potentially can be used as an indicator of  
818 river run-off (Fritz-Endres *et al.*, 2022; Hönisch *et al.*, 2011; Weldeab *et al.*, 2014). Although  
819 floods in the catchment area of the GOA are brief and occur only few times each year (Katz *et*  
820 *al.*, 2015), significant Ba/Ca perturbations during water column mixing may reflect nutrient-  
821 rich water admixing to the surface water (Fig. 7).

Deleted: 8

822 5. Discussion:

Formatted: Outline numbered + Level: 1 + Numbering  
Style: 1, 2, 3, ... + Start at: 1 + Alignment: Left + Aligned at:  
0.63 cm + Indent at: 1.27 cm

828

## 829        5.1 Temporal and vertical dynamics of element/Ca in the GOA

830        Trace element incorporation into the calcium carbonate shells of planktic foraminifera during  
 831        calcification is controlled by environmental and ecological factors in the water column such as  
 832        temperature, salinity, pH, the carbonate system, dust and terrigenous inputs, as well as whether  
 833        a species harbor photosymbionts (Schiebel & Hemleben, 2017; and others). Shells of *G. ruber*  
 834        *albus*, *T. clarkei* ‘big’ and *T. clarkei* ‘encrusted’ from the GOA show species-specific behavior  
 835        and offer new insights into how these species respond to the vertical and temporal variations  
 836        in the water column. For most elements, the smaller *T. clarkei* specimens display higher trace  
 837        element ratios than the larger *G. ruber albus*, suggesting more efficient trace element  
 838        incorporation to the shell or implying that its habitat deeper in the water column has conditions  
 839        which result in higher trace element incorporation (Fig. 8). Some element ratios such as Mg/Ca,  
 840        Sr/Ca, B/Ca, Na/Ca (for *G. ruber albus*) and Ba/Ca for both *G. ruber albus* and *T. clarkei*  
 841        ‘encrusted’, show overlap between specimens from the water column and from core-tops (Fig.  
 842        8), confirming the robustness of downcore-based records allowing to further consider these  
 843        element/Ca recorders of the water column as paleo-proxies.

844        While water depth likely influences element/Ca through variations in physical and  
 845        chemical conditions, the observed inter-chamber variability (ICV) and element/Ca differences  
 846        between species cannot be attributed to any single environmental parameter. Nonetheless,  
 847        elements such as Al/Ca, Ti/Ca, Mn/Ca, and Fe/Ca for all species, and Mg/Ca, Sr/Ca, Na/Ca,  
 848        and Ba/Ca for *G. ruber albus* alone, demonstrate consistent behavior across the water column,  
 849        suggesting that depth-related factors do not significantly alter calcification mechanisms. This  
 850        supports the use of pooled mean values for specimens over multiple sediment traps spread over  
 851        depths (Levy et al., 2023). Interestingly, most element/Ca peak during water column mixing in  
 852        March-April 2015 for all three morphotypes analyzed here, accompanied by larger ICV (Figs.  
 853        3-7). Mg/Ca in *G. ruber albus* and Sr/Ca in all three morpho-species show less pronounced  
 854        excursions, while other trace element ratios (e.g., Co/Ca, U/Ca) exhibit more variability and  
 855        more extreme values (Figs. S5 and S10). These observations can reflect: i) primary calcite  
 856        structure alterations driven by environmental shifts and life cycle changes, ii) secondary  
 857        mineralization (e.g., barite, Amorphous Calcium Carbonate, ACC) (Torres et al., 2010; Evans  
 858        et al., 2020 and references therein), and iii) fluid inclusions within the shell structure (Gray et  
 859        al., 2023).

860        All of these relationships do possibly concern the ontogenetic PF calcite, since SEM  
 861        imaging of GOA specimens did not reveal secondary minerals or overgrowth on shell calcite

Deleted: 3

Deleted: 3

Deleted: 4

Deleted: 8

866 (Levy et al., 2023). Moreover, the enrichment of multiple trace elements across species  
867 suggests that secondary minerals are unlikely to be responsible for these trends. Discrepancies  
868 between Na/Ca in plankton tow versus core-top samples in the Red Sea (Mezger et al., 2018),  
869 as well as higher Na/Ca values measured by LA-ICP-MS compared to solution ICP-MS, have  
870 been linked to early diagenesis of Na-enriched phases like spines, ACC, or fluid inclusions  
871 (Gray et al., 2023). However, spines and ACC were ruled out for GOA samples, as all of the  
872 specimens had lost their spines before analysis and ACC was not detected via SEM. Given that  
873 most element/Ca in GOA shells are elevated relative to PF data from elsewhere, fluid inclusions  
874 may be a contributing factor (Gray et al., 2023). However, more research is required to  
875 investigate whether fluid inclusions are evident in PF shells from the GOA. In the absence of  
876 fluid inclusions, environmental changes, particularly during water column mixing, are  
877 considered to be the primary drivers of the observed trace element/Ca enrichments in the GOA.  
878

## 879 5.2 Water column and sediment signal correlation: Implications to Paleoceanographic 880 studies

881 Several element ratios (e.g., Al/Ca, Ti/Ca, Mn/Ca, Fe/Ca, Nd/Ca, U/Ca, Co/Ca, and Th/Ca)  
882 exhibit discrepancies between water column and core-top specimens (Fig. 8). Some, like  
883 Co/Ca, have lower values in surface sediment than the water column, while others, like Fe/Ca  
884 show higher values. Differences between sediment trap samples and core-top samples may  
885 stem from differential diagenetic processes that affect element/Ca in specimens taken from the  
886 water column and the sea floor. For example, diagenetic processes can lead to Mn accumulation  
887 and higher Mn/Ca in PF from the core top (McKenzie, 1980; Steiner et al., 2017). Conversely,  
888 core-top PF samples may show lower ratios due to the release of these metals into pore water  
889 over time (e.g., Co/Ca, Fig. 8i). This release can alter the elemental composition, potentially  
890 skewing paleoenvironmental reconstructions. Understanding these processes is crucial for  
891 accurately interpreting geochemical data from both sample types.

892 Despite the offsets of Al/Ca and Ti/Ca between core top and water column specimens, they  
893 nevertheless may be utilized to trace the origins of terrigenous inputs and identify periods of  
894 dust deposition in the geological record (Torfstein et al., 2017; Martinez-Garcia et al., 2011).  
895 Our data reveal significant seasonal excursions in Al/Ca and may demonstrate the use of Al/Ca  
896 and Ti/Ca in PF tests as proxies for dust or terrigenous input to the ocean (Fig. S3).

897 Core top element/Ca values that fall within the same range of values of the sediment trap  
898 specimens (Mg/Ca, Sr/Ca, B/Ca, Na/Ca, and Ba/Ca; Fig. 8) suggest that they could reflect  
899 water column conditions. The high temporal variability in many of these element/Ca data,

Deleted: 3

Deleted: 3i

Deleted: 3

903 together with the varying PF population dynamics throughout the year (Fig. 2) may be  
904 considered when approaching PF from sediment cores. Seasonal trends in element/Ca are often  
905 obscured by the spring mixing event. However, exceptions to this are observed in Mg/Ca for  
906 *G. ruber albus* (Fig. 4; Levy et al., 2023) and B/Ca for *T. clarkei* (Fig. 5), where clear seasonal  
907 patterns emerge. A key limitation of reconstructing past environments from element/Ca in PF  
908 shells is the challenge of disentangling seasonal effects from other more episodic  
909 environmental signals. However, by identifying water column mixing events through positive  
910 element/Ca excursions and elevated ICV, which are evident across all species (Figs. 3-7), it  
911 may be possible to identify the time intervals over which environmental changes are  
912 reconstructed. This could allow for more accurate reconstructions of shifts in temperature,  
913 carbonate chemistry, and nutrient availability during specific mixing events, improving our  
914 understanding of past ocean conditions.

915

### 916 5.3 Regional comparison of geochemical conditions and PF element/Ca

917 The Mg/Ca, Al/Ca, and Na/Ca in PF from the GOA generally exceed those reported from other  
918 regions (Fig. 12b – 12e). Sr/Ca values, while reaching up to 2.2 mmol/mol during spring, have  
919 an average of 1.5 mmol/mol, consistent with previous studies (Fig. 12c; Kisakürek et al., 2008;  
920 Cleroux et al., 2008; Elderfield et al., 2002; Brown & Elderfield, 1996; Dissard et al., 2021).  
921 The high Mg/Ca range in the GOA versus typical open-ocean levels (0.5-5  $\mu$ mol/mol) is  
922 attributed to elevated salinity (~ 41 compared to mean ocean values of 34.7), which is also  
923 evident by the high Na/Ca. The high Al/Ca values and their large variation may be attributed  
924 to the close proximity of GOA to terrestrial input. Ba/Ca in the GOA are significantly higher  
925 than the values reported in prior studies from Atlantic Ocean core samples and culture  
926 experiments (Hönisch et al., 2011; Lea & Boyle, 1991), representing a roughly ten-fold  
927 difference. These discrepancies likely stem from two factors: (1) higher salinity in the GOA  
928 increases the availability of cations and trace element incorporation into foraminifera shells,  
929 and (2) higher-resolution measurements here which reveal chamber-specific elemental ratios,  
930 where early chambers (F-1 and F-2) exhibit higher values than final chambers, leading to more  
931 accurate, chamber-level data compared to bulk measurements. Combined, these factors explain  
932 the elevated values relative to global reports.

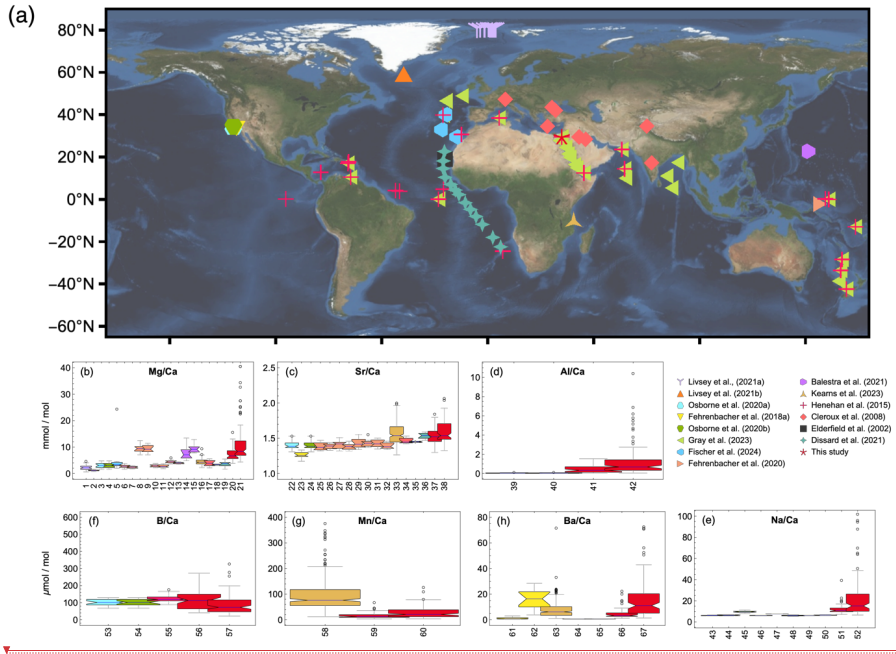
Deleted: 6

Deleted: three

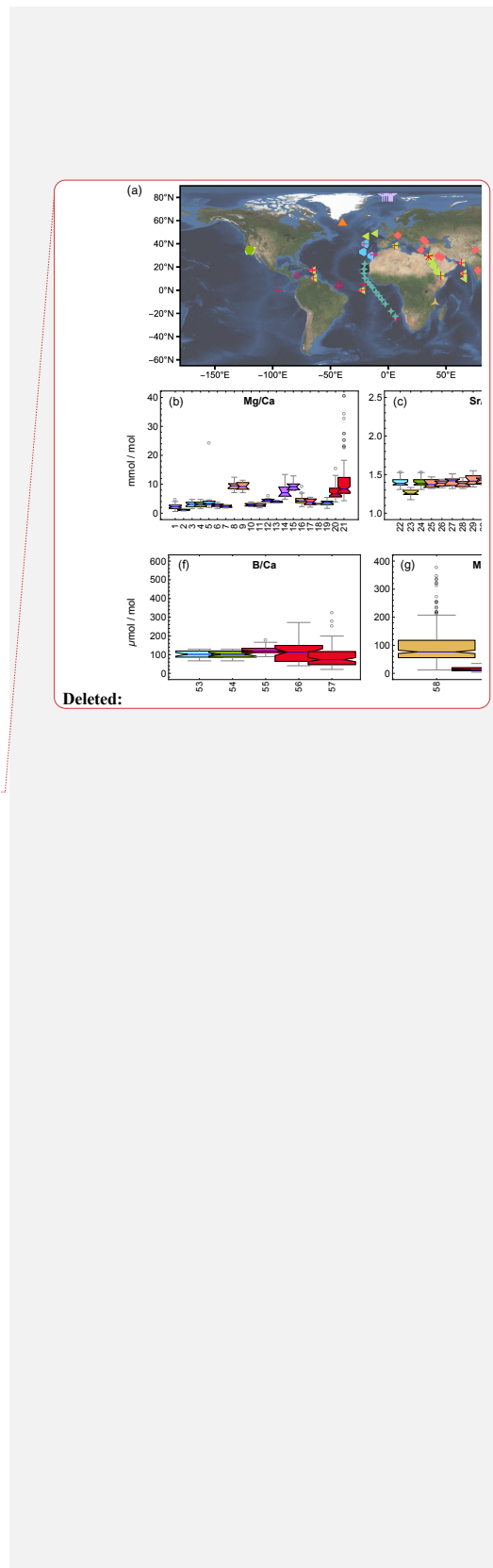
Deleted: 4

Deleted: 8

Deleted: 14e



940 Figure 12. Global comparison of major and trace element-to-calcium ratios. (a) sample global  
941 map, (b) Mg/Ca of *N. pachyderma*, *G. bulloides*, *G. ruber white*, *N. dutertrei*, *O. universa*, *P.*  
942 *obliquiloculata*, *T. sacculifer* and *T. clarkei* derived from various sources (plankton tows/nets,  
943 sediment traps, cores) and measured by Laser Ablation (LA)-ICP-MS, solution-ICP-MS (SOL)  
944 and Electron micro-probe analyses (EPMA). (c) Sr/Ca of *G. bulloides*, *G. ruber white*, *N.*  
945 *dutertrei*, *O. universa*, *P. obliquiloculata*, *T. sacculifer* and *T. clarkei* derived from various  
946 sources (plankton tows/nets, sediment traps, cores) and measured by LA-ICP-MS and solution-  
947 ICP-MS. (d) Al/Ca of *G. bulloides*, *G. ruber white* and *T. clarkei* derived from sediment traps  
948 and measured by LA-ICP-MS. (e) Na/Ca of *G. ruber white* and *T. clarkei* from various sources  
949 (plankton tows/nets, sediment traps, cores and cultured samples) and measured by LA-ICP-MS  
950 and solution-ICP-MS. (f) B/Ca of *G. bulloides*, *G. ruber white* and *T. clarkei* derived from  
951 sediment traps and measured by LA-ICP-MS. (g) Mn/Ca of *G. ruber white* and *T. clarkei*  
952 derived from cores and sediment traps and measured by LA-ICP-MS. (h) Ba/Ca of *G. ruber*  
953 white, *N. dutertrei* and *T. clarkei* derived from various sources (plankton tows/nets, sediment  
954 traps, cores and cultured samples) and measured by LA-ICP-MS. See table 1 for detailed  
955 description of methods.



957  
958

#	Element/Ca	Reference	Species	Collecting method	Measuring method
1	Mg/Ca	Livsey et al. (2021a)	<i>N. pachyderma</i>	Plankton tows / nets	LA
2	Mg/Ca	Livsey et al. (2021b)	<i>N. pachyderma</i>	Sediment traps	LA
3	Mg/Ca	Osborne et al. (2020)	<i>G. bulloides</i>	Sediment trap	LA
4	Mg/Ca	Osborne et al. (2020b)	<i>G. bulloides</i>	Sediment trap	LA
5	Mg/Ca	Fischer et al. (2024)	<i>G. ruber</i>	Plankton tows / nets	LA
6	Mg/Ca	Fehrenbacher et al. (2020)	<i>N. dutertrei</i>	Core	LA
7	Mg/Ca	Fehrenbacher et al. 2020	<i>N. dutertrei</i>	Core	SOL
8	Mg/Ca	Fehrenbacher et al. (2020)	<i>O. universa</i>	Core	LA
9	Mg/Ca	Fehrenbacher et al. (2020)	<i>O. universa</i>	Core	SOL
10	Mg/Ca	Fehrenbacher et al. (2020)	<i>P. obliquiloculata</i>	Core	LA
11	Mg/Ca	Fehrenbacher et al. (2020)	<i>P. obliquiloculata</i>	Core	SOL
12	Mg/Ca	Fehrenbacher et al. (2020)	<i>T. sacculifer</i>	Core	LA
13	Mg/Ca	Fehrenbacher et al. (2020)	<i>T. sacculifer</i>	Core	SOL
14	Mg/Ca	Balestra et al. (2021)	<i>O. universa</i>	Plankton tows / nets	EPMA

15	Mg/Ca	Balestra et al. (2022)	<i>O. universa</i>	Plankton tows / nets	EPMA
16	Mg/Ca	Kearns et al. (2023)	<i>G. ruber</i>	Core	LA
17	Mg/Ca	Cleroux et al. (2008)	<i>G. ruber</i>	Core	SOL
18	Mg/Ca	Elderfield et al. (2002)	<i>G. ruber</i>	Core	SOL
19	Mg/Ca	Dissard et al. (2021)	<i>T. sacculifer</i>	Plankton tows / nets	LA
20	Mg/Ca	This study	<i>G. ruber</i>	Sediment trap	LA
21	Mg/Ca	This study	<i>T. clarkei</i>	Sediment trap	LA
22	Sr/Ca	Osborne et al. (2020)	<i>G. Bulloides</i>	Sediment trap	LA
23	Sr/Ca	Fehrenbacher et al. (2018a)	<i>N. dutertrei</i>	Plankton tows / nets	LA
24	Sr/Ca	Osborne et al. (2020b)	<i>G. bulloides</i>	Sediment trap	LA
25	Sr/Ca	Fehrenbacher et al. (2020)	<i>N. dutertrei</i>	Core	LA
26	Sr/Ca	Fehrenbacher et al. (2020)	<i>N. dutertrei</i>	Core	SOL
27	Sr/Ca	Fehrenbacher et al. (2020)	<i>O. universa</i>	Core	LA
28	Sr/Ca	Fehrenbacher et al. (2020)	<i>O. universa</i>	Core	SOL
29	Sr/Ca	Fehrenbacher et al. (2020)	<i>P. obliquiloculata</i>	Core	LA
30	Sr/Ca	Fehrenbacher et al. (2020)	<i>P. obliquiloculata</i>	Core	SOL
31	Sr/Ca	Fehrenbacher et al. (2020)	<i>T. sacculifer</i>	Core	LA

32	Sr/Ca	Fehrenbacher et al. (2020)	<i>T. sacculifer</i>	Core	SOL
33	Sr/Ca	Kearns et al. (2023)	<i>G. ruber</i>	Core	LA
34	Sr/Ca	Cleroux et al. (2008)	<i>G. ruber</i>	Core	SOL
35	Sr/Ca	Elderfield et al. (2002)	<i>G. ruber</i>	Core	SOL
36	Sr/Ca	Dissard et al. (2021)	<i>T. sacculifer</i>	Plankton tows / nets	LA
37	Sr/Ca	This study	<i>G. ruber</i>	Sediment trap	LA
38	Sr/Ca	This study	<i>T. clarkei</i>	Sediment trap	LA
39	Al/Ca	Osborne et al. (2020)	<i>G. Bulloides</i>	Sediment trap	LA
40	Al/Ca	Osborne et al. (2020b)	<i>G. bulloides</i>	Sediment trap	LA
41	Al/Ca	This study	<i>G. ruber</i>	Sediment trap	LA
42	Al/Ca	This study	<i>T. clarkei</i>	Sediment trap	LA
43	Na/Ca	Gray et al. (2023)	<i>G. ruber</i>	Core	SOL
44	Na/Ca	Gray et al. (2023)	<i>G. ruber</i>	Cultured	SOL
45	Na/Ca	Gray et al. (2023)	<i>G. ruber</i>	Plankton tows / nets	LA
46	Na/Ca	Gray et al. (2023)	<i>G. ruber</i>	Plankton tows / nets	SOL
47	Na/Ca	Gray et al. (2023)	<i>G. ruber</i>	Sediment trap	LA
48	Na/Ca	Gray et al. (2023)	<i>G. ruber</i>	Sediment trap	SOL
49	Na/Ca	Gray et al. (2023)	<i>G. ruber mixed</i>	Core	SOL
50	Na/Ca	Gray et al. (2023)	<i>G. ruber sl</i>	Core	SOL

51	Na/Ca	This study	<i>G. ruber</i>	Sediment trap	LA
52	Na/Ca	This study	<i>T. clarkei</i>	Sediment trap	LA
53	B/Ca	Osborne et al. (2020)	<i>G. Bulloides</i>	Sediment trap	LA
54	B/Ca	Osborne et al. (2020b)	<i>G. Bulloides</i>	Sediment trap	LA
55	B/Ca	Henehan et al. (2015)	<i>G. ruber</i>	Core	SOL
56	B/Ca	This study	<i>G. ruber</i>	Sediment trap	LA
57	B/Ca	This study	<i>T. clarkei</i>	Sediment trap	LA
58	Mn/Ca	Kearns et al. (2023)	<i>G. ruber</i>	Core	LA
59	Mn/Ca	This study	<i>G. ruber</i>	Sediment trap	LA
60	Mn/Ca	This study	<i>T. clarkei</i>	Sediment trap	LA
61	Ba/Ca	Fehrenbacher et al. (2018a)	<i>N. dutertrei</i>	Cultured	LA
62	Ba/Ca	Fehrenbacher et al. (2018a)	<i>N. dutertrei</i>	Plankton tows / nets	LA
63	Ba/Ca	Kearns et al. (2023)	<i>G. ruber</i>	Core	LA
64	Ba/Ca	Hönisch et al. (2011)	<i>G. bulloides</i>	Cultured	SOL
65	Ba/Ca	Hönisch et al. (2011)	<i>O. universa</i>	Cultured	SOL
66	Ba/Ca	This study	<i>G. ruber</i>	Sediment trap	LA
67	Ba/Ca	This study	<i>T. clarkei</i>	Sediment trap	LA

959

960 Table 1: detailed description of the different species, measurement methods and sample  
 961 origin used for the compilation in figure 12. LA stands for Laser Ablation (LA)-ICP-MS,  
 962 SOL is solution-ICP-MS and EPMA is Electron micro-probe analyses.

963

964 6. Summary and conclusions:

965 We investigated the effects of inter-chamber variability on the proxy systematics in the hyper  
966 saline oligotrophic GOA using single chamber LA ICP-MS analysis measured on two flux-  
967 dominating planktic foraminifer (PF) species *G. ruber albus* and *T. clarkei* with its two  
968 phenotypes 'big' and 'encrusted'. We observed how element/Ca varies in PF chambers as a  
969 function of environmental changes in order to then be used as proxies for past oceanic and  
970 climatic reconstruction. The results show that some element/Ca exhibit temporal and seasonal  
971 variations related to environmental conditions in the water column such as Mg/Ca in *G. ruber*  
972 *albus* as a temperature proxy, and B/Ca in *T. clarkei* as a proxy of pH. Although other  
973 element/Ca values display more limited variability (e.g., Na/Ca) they may still be of use as  
974 paleo-proxies when combined in global calibration studies.

Formatted: Outline numbered + Level: 1 + Numbering  
Style: 1, 2, 3, ... + Start at: 1 + Alignment: Left + Aligned at:  
0.63 cm + Indent at: 1.27 cm

975 Water column mixing has been shown to have a significant effect of element/Ca positive  
976 excursions in the analyzed *G. ruber albus*, and two *T. clarkei* morphotypes, which may limit  
977 the use of some element ratios as proxies, or alternatively, be used as a proxy for water column  
978 mixing. Generally, pooled-mean values of element/Ca in the PF tests in the GOA are species-  
979 specific and element-specific, and are elevated compared to other regions (e.g., Mg/Ca, Al/Ca,  
980 Na/Ca). However, the final chamber F0 is different in comparison to the preceding chambers  
981 F-1 and F-2, suggesting that the element composition of F0 may be biased and unreliable in  
982 terms of recording environmental conditions.

983 Our findings indicate that high-resolution analytical techniques, such as LA ICP-MS  
984 enable studying single chamber compositions and variations. Although pooled mean values of  
985 specimens over various water depths are recommended for their incorporation as proxies, ICV  
986 can also be used as a tracer of environmental factors. Exploring different biochemical or  
987 physiological mechanisms which are responsible for the element/Ca variations between species  
988 and chambers are critical to shed light on how element/Ca are incorporated to the PF shells.  
989 Despite these limitations, the results provide valuable insights into the complex behavior of  
990 element/Ca in PF shells.

991 Data availability

992 Tabular supplementary data generated in this study can be found [in the supplementary](#)  
993 [material](#).

Deleted: at PANGAEA (DOI: will be added following  
acceptance)...

996

997 Author contributions

998 NL, AT, and RS designed the study; NL, BS, UW, and KPJ, performed the measurements;

999 NL, NC, AT, and RS analyzed the data; NL, RS and AT wrote the manuscript draft; NL, RS,

1000 AT and GH reviewed and edited the manuscript.

1001

1002 The authors declare that they have no conflict of interest.

1003

1004 Acknowledgments

1005 We wish to acknowledge the IUI marine crew and B. Yarden for their assistance in field work

1006 and sample handling. The National Monitoring Program are thanked for their support and

1007 sharing results and E. Levy for fruitful discussions. We are thankful for the three anonymous

1008 reviewers whom their comments significantly improved this manuscript. This work was

1009 supported by Israel Science Foundation grant ~~809/24~~ (to AT), a Minerva PhD Fellowship

1010 stipend (to NL) and a scholarship from the Advance School for Environmental Studies, HUJI

1011 (to NL).

1012

1013

Deleted: 834

Deleted: 19

## 1016 References

1017 Allen, K. A., Hönisch, B., Eggins, S. M., Haynes, L. L., Rosenthal, Y., & Yu, J. Trace element  
1018 proxies for surface ocean conditions: A synthesis of culture calibrations with planktic  
1019 foraminifera. *Geochim Cosmochim Ac*, 193, 197-221. (2016).

1020

1021 Allen, K. A., Hönisch, B., Eggins, S. M., Yu, J., Spero, H. J., & Elderfield, H. Controls on  
1022 boron incorporation in cultured tests of the planktic foraminifer *Orbulina universa*. *Earth*  
1023 *Planet Sc Lett*, 309(3-4), 291-301. (2011).

1024

1025 Allen, K. A., Hönisch, B., Eggins, S. M., & Rosenthal, Y. Environmental controls on B/Ca in  
1026 calcite tests of the tropical planktic foraminifer species *Globigerinoides ruber* and  
1027 *Globigerinoides sacculifer*. *Earth Planet Sc Lett*, 351, 270-280. (2012).

1028

1029 Anderson, R. F., Bacon, M. P., & Brewer, P. G. Removal of  $^{230}\text{Th}$  and  $^{231}\text{Pa}$  from the open  
1030 ocean. *Earth Planet Sc Lett*, 62(1), 7-23. (1983).

1031

1032 Babilia, T. L., Rosenthal, Y., & Conte, M. H. Evaluation of the biogeochemical controls on  
1033 B/Ca of *Globigerinoides ruber* white from the Oceanic Flux Program, Bermuda. *Earth Planet*  
1034 *Sc Lett*, 404, 67-76. (2014).

1035

1036 Balestra, B., Rose, T., Fehrenbacher, J., Knobelspiesse, K. D., Huber, B. T., Gooding, T., &  
1037 Paytan, A. In Situ Mg/Ca Measurements on Foraminifera: Comparison Between Laser  
1038 Ablation Inductively Coupled Plasma Mass Spectrometry and Wavelength-Dispersive X-Ray  
1039 Spectroscopy by Electron Probe Microanalyzer. *Geochem Geophys Geosy*, 22(2),  
1040 e2020GC009449. (2021).

1041

1042 Bé, A. W., Hemleben, C., Anderson, O. R., Spindler, M., Hacunda, J., & Tuntivate-Choy, S.  
1043 Laboratory and field observations of living planktonic foraminifera. *Micropaleontology*, 155-  
1044 179. (1977).

1045

1046 Beasley, C., Kender, S., Giosan, L., Bolton, C. T., Anand, P., Leng, M. J., Nilsson-Kerr k.,  
1047 Ullmann C. V., Hesselbo S. P., & Littler, K. Evidence of a South Asian proto-monsoon during  
1048 the Oligocene-Miocene transition. *Paleoceanogr Paleoclimatol*, 36(9), e2021PA004278.  
1049 (2021).

1050 Berggren, W. A., Kent, D. V., Swisher, C. C., & Aubry, M. P. A revised Cenozoic  
1051 geochronology and chronostratigraphy. (1995).

1052

1053 Bertlich, J., Nürnberg, D., Hathorne, E. C., De Nooijer, L. J., Mezger, E. M., Kienast, M.,  
1054 Nordhausen S., Reichart G., Schönfeld J., & Bijma, J. Salinity control on Na incorporation into  
1055 calcite tests of the planktonic foraminifera *Trilobatus sacculifer*—evidence from culture  
1056 experiments and surface sediments. *Biogeosciences*, 15(20), 5991-6018. (2018).

1057

1058 Bolton, A., Baker, J. A., Dunbar, G. B., Carter, L., Smith, E. G., & Neil, H. L. Environmental  
1059 versus biological controls on Mg/Ca variability in *Globigerinoides ruber* (white) from core top  
1060 and plankton tow samples in the southwest Pacific Ocean. *Paleoceanography*, 26(2). (2011).

1061 Brummer, G. J. A., & Kučera, M. Taxonomic review of living planktonic foraminifera. *J*  
1062 *Micropalaeontol*, 41(1), 29-74. (2022).

1063 Brown, S. J., & Elderfield, H. Variations in Mg/Ca and Sr/Ca ratios of planktonic foraminifera  
1064 caused by postdepositional dissolution: Evidence of shallow Mg-dependent  
1065 dissolution. *Paleoceanography*, 11(5), 543-551. (1996).

1066

1067 Chang, F., Li, T., Xiong, Z., & Xu, Z. Evidence for sea level and monsoonally driven variations  
1068 in terrigenous input to the northern East China Sea during the last 24.3  
1069 ka. *Paleoceanography*, 30(6), 642-658. (2015).

1070

1071 Chase, Z., Paytan, A., Beck, A., Biller, D., Bruland, K., Measures, C., & Sañudo-Wilhelmy, S.  
1072 Evaluating the impact of atmospheric deposition on dissolved trace-metals in the Gulf of  
1073 Aqaba, Red Sea. *Mar Chem*, 126(1-4), 256-268. (2011).

1074

1075 Chernihovsky, N., Torfstein, A., & Almogi-Labin, A. Seasonal flux patterns of planktonic  
1076 foraminifera in a deep, oligotrophic, marginal sea: Sediment trap time series from the Gulf of  
1077 Aqaba, northern Red Sea. *Deep-Sea Res Pt I*, 140, 78-94. (2018).

1078

1079 Chernihovsky, N., Almogi-Labin, A., Kienast, S. S., & Torfstein, A. The daily resolved  
1080 temperature dependence and structure of planktonic foraminifera blooms. *Sci Rep-Uk*, 10(1),  
1081 17456. (2020).

1082

1083 Cléroux, C., Cortijo, E., Anand, P., Labeyrie, L., Bassinot, F., Caillon, N., & Duplessy, J. C.

1084 Mg/Ca and Sr/Ca ratios in planktonic foraminifera: Proxies for upper water column

1085 temperature reconstruction. *Paleoceanography*, 23(3). (2008).

1086

1087 Costa, K. M., Hayes, C. T., Anderson, R. F., Pavia, F. J., Bausch, A., Deng, F., Dutay, J.,

1088 Geibert, W., Heinze, C., Henderson, G., Hillaire-Marcel, C., Hoffmann, S., Jaccard, S. L.,

1089 Jacobel, A. W., Kienast, S. S., Kipp, L., Lerner, P., Lippold, J., Lund, D., Marcantonio, F.,

1090 McGee, D., McManus, J. F., Mekik, F., Middleton, J. L., Missiaen, L., Not, C., Pichat, S.,

1091 Robinson, L. F., Rowland, G. H., Roy-Barman, M., Tagliabue, A., Torfstein, A., Winckler, G.,

1092 & Zhou, Y. 230Th normalization: New insights on an essential tool for quantifying sedimentary

1093 fluxes in the modern and Quaternary ocean. *Paleoceanogr Paleoclimatol*, 35(2),

1094 e2019PA003820. (2020).

1095

1096 Davis, C. V., Fehrenbacher, J. S., Benitez-Nelson, C., & Thunell, R. C. Trace element

1097 heterogeneity across individual planktic foraminifera from the Modern Cariaco Basin. *J*

1098 *Foramin Res*, 50(2), 204-218. (2020).

1099

1100 Dissard, D., Reichart, G. J., Menkes, C., Mangeas, M., Frickenhaus, S., & Bijma, J. Mg/Ca,

1101 Sr/Ca and stable isotopes from the planktonic foraminifera *T. sacculifer*: testing a multi-proxy

1102 approach for inferring paleotemperature and paleosalinity. *Biogeosciences*, 18(2), 423-439.

1103 (2021).

1104

1105 [Eggins, S., De Deckker, P., & Marshall, J. \(2003\). Mg/Ca variation in planktonic foraminifera](#)

1106 [tests: implications for reconstructing palaeo-seawater temperature and habitat migration. \*Earth\*](#)

1107 [and Planetary Science Letters](#), 212(3-4), 291-306.

1108

1109 Elderfield, H., Vautravers, M., & Cooper, M. The relationship between shell size and Mg/Ca,

1110 Sr/Ca,  $\delta^{18}\text{O}$ , and  $\delta^{13}\text{C}$  of species of planktonic foraminifera. *Geochim Geophys Geosy*, 3(8),

1111 1-13. (2002).

1112 Evans, D., Gray, W. R., Rae, J. W., Greenop, R., Webb, P. B., Penkman, K., Kröger, R., &

1113 Allison, N. Trace and major element incorporation into amorphous calcium carbonate (ACC)

1114 precipitated from seawater. *Geochim Cosmochim Ac*, 290, 293-311. (2020).

1115

1116 Fehrenbacher, J., Marchitto, T., & Spero, H. J. Comparison of Laser Ablation and Solution-  
1117 Based ICP-MS Results for Individual Foraminifer Mg/Ca and Sr/Ca Analyses. *Geochim  
1118 Geophys Geosy*, 21(12), e2020GC009254. (2020).

1119

1120 Fehrenbacher, Jennifer; Russell, Ann D; Davis, Catherine V; Spero, Howard J; Chu, Edward;  
1121 Hönnisch, Bärbel: Average barium/calcium ratios of cultured foraminifer specimens of  
1122 *Neogloboquadrina dutertrei*, listed by experiment  
1123 [dataset]. PANGAEA, <https://doi.org/10.1594/PANGAEA.895792>, (2018).

1124

1125 Fischer, A., Schiebel, R., Jochum, K. P., Heins, L., Arns, A. I., Aardema, H. M., Slagter, H.,  
1126 Calleja, M. L., Levy, N., Stoll, B., Weis, U., Repschläger, J., & Haug, G. H. Single chamber  
1127 Mg/Ca analyses of *Globigerinoides ruber* for paleo-proxy calibration using femtosecond LA-  
1128 ICP-MS. *Sci. Data*, 11(1), 583. (2024).

1129

1130 Francois, R., Frank, M., Rutgers van der Loeff, M. M., & Bacon, M. P. 230Th normalization:  
1131 An essential tool for interpreting sedimentary fluxes during the late  
1132 Quaternary. *Paleoceanography*, 19(1). (2004).

1133

1134 Fritz-Endres, T., Fehrenbacher, J. S., Russell, A. D., & Cynar, H. Increased productivity in the  
1135 equatorial pacific during the deglaciation inferred from the Ba/Ca ratios of non-spinose  
1136 planktic foraminifera. *Paleoceanogr Paleoclimatol*, 37(12), e2022PA004506. (2022).

1137

1138 Ganor, E., & Foner, H. A. Mineral dust concentrations, deposition fluxes and deposition  
1139 velocities in dust episodes over Israel. *J Geophys Res-Atmos*, 106(D16), 18431-18437. (2001).

1140

1141 Ganssen, G. M., Peeters, F. J. C., Metcalfe, B., Anand, P., Jung, S. J. A., Kroon, D., &  
1142 Brummer, G. J. Quantifying sea surface temperature ranges of the Arabian Sea for the past 20  
1143 000 years. *Clim Past*, 7(4), 1337-1349. (2011).

1144

1145 Geerken, E., De Nooijer, L. J., van Dijk, I., & Reichart, G. J. Impact of salinity on element  
1146 incorporation in two benthic foraminiferal species with contrasting magnesium  
1147 contents. *Biogeosciences*, 15(7), 2205-2218. (2018).

1148

1149 Gray, W. R., Evans, D., Henehan, M., Weldeab, S., Lea, D. W., Müller, W., & Rosenthal, Y.  
1150 Sodium incorporation in foraminiferal calcite: An evaluation of the Na/Ca salinity proxy and  
1151 evidence for multiple Na-bearing phases. *Geochim Cosmochim Ac*, 348, 152-164. (2023).

1152

1153 Gupta, B. K. S. *Modern foraminifera* (pp. 7-36). B. K. S. Gupta (Ed.). Dordrecht: Kluwer  
1154 Academic Publishers. (1999).

1155 Haug, G. H., Gunther, D., Peterson, L. C., Sigman, D. M., Hughen, K. A., & Aeschlimann, B.  
1156 Climate and the collapse of Maya civilization. *Science*, 299(5613), 1731-1735. (2003).

1157 Haynes, L. L., Hönisch, B., Holland, K., Rosenthal, Y., & Eggins, S. M. Evaluating the planktic  
1158 foraminiferal B/Ca proxy for application to deep time paleoceanography. *Earth Planet Sc  
1159 Lett*, 528, 115824. (2019).

1160 Henehan, M. J., Foster, G. L., Rae, J. W., Prentice, K. C., Erez, J., Bostock, H. C., Marshall,  
1161 B. J., & Wilson, P. A. Evaluating the utility of B/C a ratios in planktic foraminifera as a proxy  
1162 for the carbonate system: A case study of *Globigerinoides ruber*. *Geochem Geophys  
1163 Geosy*, 16(4), 1052-1069. (2015).

1164 Hönisch, B., Allen, K. A., Russell, A. D., Eggins, S. M., Bijma, J., Spero, H. J., Lea, D. W., &  
1165 Yu, J. Planktic foraminifers as recorders of seawater Ba/Ca. *Mar Micropaleontol*, 79(1-2), 52-  
1166 57. (2011).

1167 Hönisch, B., Fish, C. R., Phelps, S. R., Haynes, L. L., Dyez, K., Holland, K., Fehrenbacher, J.,  
1168 Allen, K. A., Eggins, S. M., & Goes, J. I. Symbiont photosynthesis and its effect on boron  
1169 proxies in planktic foraminifera. *Paleoceanogr Paleoclimatol*, 36(10), e2020PA004022.  
1170 (2021).

1171 Hupp, B. N., & Fehrenbacher, J. S. Intratess trace element variability in polar and subpolar  
1172 planktic foraminifera: Insights into vital effects, ontogeny, and biomineralization processes. *J  
1173 Foramin Res*, 54(4), 355-374. (2024).

1174 Israel National Monitoring Program (NMP) (<http://www.iui-ielat.ac.il/Research/NMPmeteodata.aspx>; Shaked and Genin. (2016).

1176 Jochum, K. P., Jentzen, A., Schiebel, R., Stoll, B., Weis, U., Leitner, J., Repschläger, J.,  
1177 Nürnberg, D., & Haug, G. H. High-resolution Mg/Ca measurements of foraminifer shells using  
1178 femtosecond LA-ICP-MS for paleoclimate proxy development. *Geochem Geophys Geosy*, 20(4), 2053-2063. (2019).

1180

1181 Jochum, K. P., Stoll, B., Weis, U., Jacob, D. E., Mertz-Kraus, R., & Andreae, M. O. Non-  
1182 matrix-matched calibration for the multi-element analysis of geological and environmental  
1183 samples using 200 nm femtosecond LA-ICP-MS: A comparison with nanosecond  
1184 lasers. *Geostand Geoanal Res*, 38(3), 265-292. (2014).

1185

1186 Jonkers, L., De Nooijer, L. J., Reichart, G. J., Zahn, R., & Brummer, G. J. Encrustation and  
1187 trace element composition of *Neogloboquadrina dutertrei* assessed from single chamber  
1188 analyses—implications for paleotemperature estimates. *Biogeosciences*, 9(11), 4851-4860.  
1189 (2012).

1190

1191 Katz, M. E., Cramer, B. S., Franzese, A., Hönnisch, B., Miller, K. G., Rosenthal, Y., & Wright,  
1192 J. D. Traditional and emerging geochemical proxies in foraminifera. *J Foramin Res*, 40(2),  
1193 165-192. (2010).

1194

1195 Katz, T., Ginat, H., Eyal, G., Steiner, Z., Braun, Y., Shalev, S., & Goodman-Tchernov, B. N.  
1196 Desert flash floods form hyperpycnal flows in the coral-rich Gulf of Aqaba, Red Sea. *Earth  
1197 Planet Sc Lett*, 417, 87-98. (2015).

1198

1199 Kearns, L. E., Searle-Barnes, A., Foster, G. L., Milton, J. A., Standish, C. D., & Ezard, T. H.  
1200 G. The influence of geochemical variation among *Globigerinoides ruber* individuals on  
1201 Paleoceanographic reconstructions. *Paleoceanogr Paleoclimatol*, 38(4), e2022PA004549.  
1202 (2023).

1203

1204 Kısakürek, B., Eisenhauer, A., Böhm, F., Garbe-Schönberg, D., & Erez, J. Controls on shell  
1205 Mg/Ca and Sr/Ca in cultured planktonic foraminifera, *Globigerinoides ruber* (white). *Earth  
1206 Planet Sc Lett*, 273(3-4), 260-269. (2008).

1207

1208 Kucera, M. Chapter six planktonic foraminifera as tracers of past oceanic  
1209 environments. Editor(s): Claude Hillaire-Marcel, Anne De Vernal, *Developments in marine*  
1210 *geology*, Elsevier, 1, 213-262. ISBN 9780444527554, (2007).

1211

1212 Lea, D. W., & Boyle, E. A. Barium in planktonic foraminifera. *Geochim Cosmochim Ac*, 55(11), 3321-3331. (1991).

1213

1214 Levy, N., Torfstein, A., Schiebel, R., Chernihovsky, N., Jochum, K. P., Weis, U., Stoll, B., &  
1215 Haug, G. H. Temperature calibration of elevated Mg/Ca in planktic Foraminifera shells from  
1216 the hypersaline Gulf of Aqaba. *Geochem Geophy Geosy*, 24(7), e2022GC010742. (2023).

1217

1218 Livsey, Caitlin M; Kozdon, Reinhard; Bauch, Dorothea; Brummer, Geert-Jan A; Jonkers,  
1219 Lukas; Orland, Ian; Hill, Tessa M; Spero, Howard J: In situ Magnesium/Calcium analyses by  
1220 LA-ICP-MS in individual N. pachyderma shells from plankton tows deployed in the Fram  
1221 Strait [dataset]. PANGAEA, <https://doi.org/10.1594/PANGAEA.935527>, (2021a).

1222

1223 Livsey, Caitlin M; Kozdon, Reinhard; Bauch, Dorothea; Brummer, Geert-Jan A; Jonkers,  
1224 Lukas; Orland, Ian; Hill, Tessa M; Spero, Howard J: Mg/Ca analyses by LA-ICP-MS in N.  
1225 pachyderma shells from Irminger Sea sediment traps  
1226 [dataset]. PANGAEA, <https://doi.org/10.1594/PANGAEA.935595>, (2021b).

1227

1228 Martínez-Garcia, A., Rosell-Melé, A., Jaccard, S. L., Geibert, W., Sigman, D. M., & Haug, G.  
1229 H. Southern Ocean dust-climate coupling over the past four million years. *Nature*, 476(7360),  
1230 312-315. (2011).

1231

1232 McKenzie, R. M. The adsorption of lead and other heavy metals on oxides of manganese and  
1233 iron. *Soil Res*, 18(1), 61-73. (1980).

1234

1235

1236 Meeder, E., Mackey, K. R., Paytan, A., Shaked, Y., Iluz, D., Stambler, N., Rivlin, T., Post, A.  
1237 F., & Lazar, B. Nitrite dynamics in the open ocean clues from seasonal and diurnal  
1238 variations. *Mar Ecol Prog Ser*, 453, 11-26. (2012).

1239

1240 Mesa-Fernández, J. M., Martínez-Ruiz, F., Rodrigo-Gámiz, M., Jiménez-Espejo, F. J., García,  
1241 M., & Sierro, F. J. Paleocirculation and paleoclimate conditions in the western Mediterranean  
1242 basins over the last deglaciation: New insights from sediment composition variations. *Global*  
1243 *Planet Change*, 209, 103732. (2022).

1244

1245 Mezger, E. M., de Nooijer, L. J., Boer, W., Brummer, G. J. A., & Reichart, G. J. Salinity  
1246 controls on Na incorporation in Red Sea planktonic foraminifera. *Paleoceanography*, 31(12),  
1247 1562-1582. (2016).

1248

1249 Mezger, E. M., de Nooijer, L. J., Siccha, M., Brummer, G. J., Kucera, M., & Reichart, G. J.  
1250 Taphonomic and ontogenetic effects on Na/Ca and Mg/Ca in spinose planktonic foraminifera  
1251 from the Red Sea. *Geochem Geophy Geosy*, 19(11), 4174-4194. (2018).

1252

1253 Morard, R., Füllberg, A., Brummer, G. J. A., Greco, M., Jonkers, L., Wizemann, A., Weiner,  
1254 A. K. M., Darling, K., Siccha, M., Ledevin, R., Kitazato, H., de Gardiel-Thoron, T., de Vargas,  
1255 C., & Kucera, M. Genetic and morphological divergence in the warm-water planktonic  
1256 foraminifera genus *Globigerinoides*. *PloS one*, 14(12), e0225246. (2019).

1257 Naik, S. S., & Naidu, P. D. Boron/calcium ratios in *Globigerinoides ruber* from the Arabian  
1258 Sea: Implications for controls on boron incorporation. *Mar Micropaleontol*, 107, 1-7. (2014).

1259 Nürnberg, D., Bijma, J., & Hemleben, C. Assessing the reliability of magnesium in  
1260 foraminiferal calcite as a proxy for water mass temperatures. *Geochim Cosmochim Ac*, 60(5),  
1261 803-814. (1996).

1262 Osborne, Emily B; Umling, Natalie E; Bizimis, Michael; Buckley, Wayne; Sadekov, Aleksey  
1263 Y; Tappa, Eric; Marshall-Kesser, Brittney; Sautter, Leslie R; Thunell, Robert C: Boron to  
1264 calcium ratios (B/Ca) of sediment trap collected planktonic foraminifera from the Santa  
1265 Barbara Basin [dataset publication  
1266 series]. PANGAEA, <https://doi.org/10.1594/PANGAEA.91087>, (2020a).

1267 Osborne, Emily B; Umling, Natalie E; Bizimis, Michael; Buckley, Wayne; Sadekov, Aleksey  
1268 Y; Tappa, Eric; Marshall-Kesser, Brittney; Sautter, Leslie R; Thunell, Robert C: Geochemistry  
1269 of *Globigerina* *Bulloides* in Santa Barbara Basin measured by Laser Ablation  
1270 [dataset]. PANGAEA, <https://doi.org/10.1594/PANGAEA.912273>, (2020b).

1271 Rebotim, A., Voelker, A. H., Jonkers, L., Waniek, J. J., Meggers, H., Schiebel, R., Fraile, I.,  
1272 Schulz, M., & Kucera, M. Factors controlling the depth habitat of planktonic foraminifera in  
1273 the subtropical eastern North Atlantic. *Biogeosciences*, 14(4), 827-859. (2017).

1274 [Reichart, G. J., Jorissen, F., Anschutz, P., & Mason, P. R. \(2003\). Single foraminiferal test](#)  
1275 [chemistry records the marine environment. \*Geology\*, 31\(4\), 355-358.](#)

1276  
1277 Rosenthal, Y. Chapter nineteen elemental proxies for reconstructing cenozoic seawater  
1278 paleotemperatures from calcareous fossils. Editor(s): Claude Hillaire-Marcel, Anne De  
1279 Vernal, *Developments in Marine Geology*, Elsevier, 1, 765-797. ISBN 9780444527554,  
1280 (2007).

1281  
1282 Rosenthal, Y., Perron-Cashman, S., Lear, C. H., Bard, E., Barker, S., Billups, K., Bryan, M.,  
1283 Delaney, M. L., deMenocal, P. B., Dwyer, G. S., Elderfield, H., German, C. R., Greaves, M.,  
1284 Lea, D. W., Marchitto, T. M. Jr., Pak, D. K., Paradis, G. L., Russell, A. D., Schneider, R. R.,  
1285 Scheiderich, K., Stott, L., Tachikawa, K., Tappa, E., Thunell, R., Wara, M., Weldeab, S., &  
1286 Wilson, P. A. Interlaboratory comparison study of Mg/Ca and Sr/Ca measurements in  
1287 planktonic foraminifera for paleoceanographic research. *Geochem Geophy Geosy* 5(4). (2004).

1288  
1289 Sadekov, A., Eggins, S. M., De Deckker, P., Ninnemann, U., Kuhnt, W., & Bassinot, F. Surface  
1290 and subsurface seawater temperature reconstruction using Mg/Ca microanalysis of planktonic  
1291 foraminifera *Globigerinoides ruber*, *Globigerinoides sacculifer*, and *Pulleniatina obliquiloculata*. *Paleoceanography*, 24(3). (2009).

1293  
1294 Sadekov, A., Eggins, S. M., De Deckker, P., & Kroon, D. Uncertainties in seawater  
1295 thermometry deriving from intratest and intertest Mg/Ca variability in *Globigerinoides*  
1296 *ruber*. *Paleoceanography*, 23(1). (2008).

1297  
1298 Schiebel, R., & Hemleben, C. *Planktic foraminifers in the modern ocean* (pp. 1-358). Berlin:  
1299 Springer. (2017).

1300  
1301 Shaked, Y., & Genin, A. Israel National Monitoring Program at the Gulf of Eilat Annual  
1302 Report. (2016).

1304 Spero, H. J., Mielke, K. M., Kalve, E. M., Lea, D. W. & Pak, D. K. Multispecies approach to  
1305 reconstructing eastern equatorial Pacific thermocline hydrography during the past 360 kyr.  
1306 *Paleoceanography*, 18, 1022 (2003).

1307

1308 Sprintall, J. & Tomczak, M. Evidence of the barrier layer in the surface layer of the tropics. *J*  
1309 *Geophys Res-Oceans*, 97(C5), 7305-7316. (1992).

1310

1311 Steiner, Z., Lazar, B., Torfstein, A., & Erez, J. Testing the utility of geochemical proxies for  
1312 paleoproductivity in oxic sedimentary marine settings of the Gulf of Aqaba, Red Sea. *Chem*  
1313 *Geol*, 473, 40-49. (2017).

1314

1315 Thirumalai, K., Richey, J. N., Quinn, T. M., & Poore, R. Z. Globigerinoides ruber morphotypes  
1316 in the Gulf of Mexico: A test of null hypothesis. *Scientific reports*, 4(1), 6018.

1317 Torfstein, A., Kienast, S. S., Yarden, B., Rivlin, A., Isaacs, S., & Shaked, Y. (2020). Bulk and export  
1318 production fluxes in the Gulf of Aqaba, Northern Red Sea. *ACS Earth Space Chem*, 4(8), 1461-  
1319 1479. (2014).

1320

1321 Torfstein, A., Teutsch, N., Tirosh, O., Shaked, Y., Rivlin, T., Zipori, A., Stein, M., Lazar, B.,  
1322 & Erel, Y. Chemical characterization of atmospheric dust from a weekly time series in the  
1323 north Red Sea between 2006 and 2010. *Geochim Cosmochim Ac*, 211, 373-393. (2017).

1324

1325 Torres, M. E., Martin, R. A., Klinkhammer, G. P., & Nesbitt, E. A. Post depositional alteration  
1326 of foraminiferal shells in cold seep settings: new insights from flow-through time-resolved  
1327 analyses of biogenic and inorganic seep carbonates. *Earth Planet Sc Lett*, 299(1-2), 10-22.  
1328 (2010).

1329

1330 Weldeab, S., Lea, D. W., Oberhaensli, H. & Schneider, R. R. Links between southwestern  
1331 tropical Indian Ocean SST and precipitation over southeastern Africa over the last 17 kyr.  
1332 *Palaeogeogr Palaeoocl*. 410, 1-13 (2014).

1333

1334 Yu, J., Elderfield, H., & Hönisch, B. B/Ca in planktonic foraminifera as a proxy for surface  
1335 seawater pH. *Paleoceanography*, 22(2). (2007).